

---

*Instrumentation Development,  
Measurement and Performance  
Evaluation of Environmental  
Technologies*

**Quarterly Technical Progress Report  
for the period  
July 1, 2000 - September 30, 2000**

**Dr. John Plodinec, Principal Investigator**

**Report No. 40395R09**

**Prepared for the U.S. Department of Energy  
Agreement No. DE-FC26-98FT40395**

**Diagnostic Instrumentation and Analysis Laboratory  
Mississippi State University  
205 Research Boulevard  
Starkville, Mississippi 39759-9734**

**dial@dial.msstate.edu  
www.msstate.edu/Dept/DIAL**

---

**Notice**

This report was prepared as an account of work sponsored by an agency of the United States Government. Neither the United States Government nor any agency thereof, nor any of their employees, makes any warranty, express or implied, or assumes any legal liability or responsibility for the accuracy, completeness, or usefulness of any information, apparatus, product or process disclosed or represents that its use would not infringe privately-owned rights. Reference herein to any specific commercial product, process, or service by trade name, trademark, manufacturer, or otherwise does not necessarily constitute or imply its endorsement, recommendation, or favoring by the United States Government or any agency thereof. The views and opinions of authors expressed therein do not necessarily state or reflect those of the United States Government or any agency thereof.

# *Table of Contents*

Executive Summary .....	1
Characterization of Heavy Metals, Radionuclides and Organics in Heterogeneous Media. ....	1
Environmental Control Device Testing .....	2
Waste Treatment and D&D Support: Process Monitoring And Control. ....	4
Diagnostic Field Applications Coordination and Testing Support (DFACTS) .....	8
 TASK 1 Characterization of Heavy Metals, Radionuclides and Organics in Heterogeneous Media. ....	 10
Volatile Organic Compound Monitoring Using Diode Lasers. ....	 10
Sensitive Detection of Toxic Chlorinated Compounds ..	15
Isotopically Selective Monitors for Transuranic Elements .....	17
Laser-induced Breakdown Spectroscopy .....	25
 TASK 2 Environmental Control Device Testing. ....	 30
Performance Enhancement of the Ionizing Wet Scrubber .....	 30
Testing of a Ceramic Regenerative Heat Storage Device for Dioxin Control and Heat Recovery .....	32
TranSportable Calibration Test Stand for Diagnostic Instrumentation. ....	36
Evaluation and Performance Enhancement of a Submerged Bed Scrubber. ....	39

TASK 3	Waste Treatment and D&D Support: Process Monitoring and Control . . . . .	42
	Dioxin and PCB Studies . . . . .	42
	On-line Multi-Spectral Imaging of Thermal Treatment Processes . . . . .	46
	On-line Monitor for Gall Layer Detection . . . . .	51
	Imaging Instrumentation Application and Development: Thermal Imaging. . . . .	52
	Imaging Instrumentation Application and Development: Profilometry . . . . .	54
	Saltcake Dissolution . . . . .	56
	Solids Formation. . . . .	85
TASK 4	Diagnostic Field Applications Coordination and Testing Support (DFACTS) . . . . .	125
	HEPA Filter Testing . . . . .	125

## *List of Figures*

FIGURE 1	Comparison of ringdown waveforms with/without a VOC sample in the cell. . . . .	13
FIGURE 2	Calibration graph for chlorobenzene obtained with the DL-CRDS system. . . . .	13
FIGURE 3	Schematic of cavity ringdown spectroscopy (CRDS) apparatus . . . . .	21
FIGURE 4	Schematic of the laser-induced fluorescence spectrometry technique . . . . .	22
FIGURE 5	Schematic of isotopic energy shifts and the associated LIF spectrum. . . . .	22
FIGURE 6	LIBS signal obtained at different LTSD from a glass sample . . . . .	27
FIGURE 7	Aluminum calibration for Fe . . . . .	28
FIGURE 8	Schematic of the transportable calibration test stand for diagnostic instrumentation . . . . .	37
FIGURE 9	Scale model of West Valley submerged bed scrubber. . . . .	40
FIGURE 10	Spectral images of a cotton leaf at four different wavelengths. . . . .	49
FIGURE 11	Ratio image of a cotton leaf for 700-nm image/760-nm image and the histogram of the selected area on the leaf . . . . .	49
FIGURE 12	Prior (FY 99) comparison of predicted and experimental nitrate anion concentrations for Tank S-102 . . . . .	63
FIGURE 13	Comparison of ESP prediction and experimental data for sulfate anion from series dissolution tests on TX-113 saltcake, 25°C . . . . .	67
FIGURE 14	Comparison of ESP prediction and experimental data for sulfate anion series dissolution tests on TX-113 saltcake, 25°C, incorporation of Na <sub>2</sub> SO <sub>4</sub> database. . . . .	68
FIGURE 15	ESP predictions and experimental nitrate concentrations for TX-113 Saltcake at 25°C . . . . .	70

FIGURE 16	ESP predictions and experimental nitrate concentrations for TX-113 saltcake at 50°C . . . . .	71
FIGURE 17	ESP predictions and experimental TIC concentrations for TX-113 saltcake at 25°C . . . . .	72
FIGURE 18	ESP predictions and experimental TIC concentrations for TX-113 saltcake at 50°C . . . . .	72
FIGURE 19	ESP predictions and experimental sulfate concentrations for TX-113 saltcake at 50°C . . . . .	76
FIGURE 20	ESP predictions and experimental fluoride concentrations for TX-113 saltcake at 25°C . . . . .	77
FIGURE 21	ESP predictions and experimental fluoride concentrations for TX-113 saltcake at 50°C . . . . .	78
FIGURE 22	ESP predictions and experimental phosphate concentrations for TX-113 saltcake at 25°C . . . . .	79
FIGURE 23	ESP predictions and experimental phosphate concentrations for TX-113 saltcake at 50°C . . . . .	79
FIGURE 24	ESP predictions and experimental nitrite concentrations for TX-113 saltcake at 25°C . . . . .	80
FIGURE 25	ESP predictions and experimental nitrite concentrations for TX-113 saltcake at 50°C . . . . .	81
FIGURE 26	ESP model predictions and experimental chloride concentrations for TX-113 saltcake at 25°C . . . . .	81
FIGURE 27	ESP predictions and experimental chloride concentrations for TX-113 saltcake at 50°C . . . . .	82
FIGURE 28	ESP model predictions and experimental oxalate concentrations for TX-113 saltcake at 25°C . . . . .	82
FIGURE 29	ESP predictions and experimental oxalate concentrations for TX-113 saltcake at 50°C . . . . .	83
FIGURE 30	Viscosity against shear rate traces for the sample 8 surrogate . . . . .	88
FIGURE 31	Pressures and temperatures recorded for the experiment on 8/22/00 . . . . .	91
FIGURE 32	Pressures for the experiments at different flow rates . . . . .	94
FIGURE 33	Temperatures for the experiments at different Reynolds numbers . . . . .	95
FIGURE 34	Model flow chart . . . . .	103

FIGURE 35	View of the straight pipe segment ( $L = 12.9$ and $D = 0.0275$ meters) and the grid used, enlarged 50 times in the radial direction . . . . .	113
FIGURE 36	Density distribution along the transfer pipe center line as a function of flow velocity at the entrance, $U = 0.5, 0.8, 1.1, 1.2$ and $2.5$ meters/sec . . . . .	114
FIGURE 37	Carrier fluid concentration along the transfer pipe center line as a function of flow velocity at the entrance, $U = 0.5, 0.8, 1.1, 1.2$ and $2.5$ meters/sec . . . . .	115
FIGURE 38	$400 \mu$ particle concentration along the transfer pipe center line as a function of flow velocity at the entrance, $U = 0.5, 0.8, 1.1, 1.2$ and $2.5$ meters/sec . . . . .	115
FIGURE 39	$45 \mu$ particle concentration along the transfer pipe center line as a function of flow velocity at the entrance, $U = 0.5, 0.8, 1.1, 1.2$ and $2.5$ meters/sec . . . . .	116
FIGURE 40	Density distribution along the transfer pipe center line (top), across the transfer pipe line at suspected plug location (center) and at $x = 6.45$ meters in the axial direction . . . . .	117
FIGURE 41	Density distribution along the transfer pipe center line (top), across the transfer pipe line at suspected plug location (center) and at $x = 6.45$ meters in the axial direction . . . . .	118

## *List of Tables*

TABLE 1	Major constituents in saltcakes examined (weight percent of sample) . . . . .	59
TABLE 2	Molecular streams for TX-113 and S-102 saltcakes generated using revised strategy for pre-processing of low water content saltcakes (units are molality). . . . .	64
TABLE 3	Comparison of solid phase speciation - inclusion of $\text{Na}_6(\text{SO}_4)_2\text{CO}_3$ as potential solid. . . . .	75
TABLE 4	Locations of thermocouples (T) and pressure transducers (P) along the channel. . . . .	89
TABLE 5	Characteristics of the initial experiments . . . . .	92
TABLE 6	Average values for the experimental conditions . . . . .	92
TABLE 7	Characteristics of FIU slurry C . . . . .	111
TABLE 8	Entrance flow velocity for simulation cases . . . . .	114

---

## *Executive Summary*

---

---

### ***Characterization of Heavy Metals, Radionuclides and Organics in Heterogeneous Media***

**Volatile organic compound monitoring using diode lasers.** A significant number of DOE needs are associated with applications requiring small, robust, and sensitive sensors for toxic volatile organic compounds (VOCs). This report describes our progress in developing diode laser cavity ringdown spectroscopy (DL-CRDS) for VOC monitoring. During the last quarter, a new sample introduction system was constructed and used to obtain quantitative absorption measurements of chlorobenzene in the DL-CRDS system. At present, the detection capabilities of the system correspond to a detection limit of 200 ppb for chlorobenzene. Improvements aimed at improving the system reproducibility and the detection limit are described.

**Sensitive detection of toxic chlorinated compounds.** The near ultraviolet absorption spectrum of 2-chloro-dibenzo-*p*-dioxin at ambient temperature has been obtained in the 260 - 310-nm region by cavity ring-down spectroscopy. This is the first cavity ring-down spectrum for a chlorinated dioxin species.

**Isotopically selective monitors for transuranic elements.** During the past quarter, cavity ringdown experiments have focused on achieving a better understanding of the interaction between the ICP plasma and

the stable modes of the ringdown cavity. Developing an understanding of the physical mechanisms of the plasma's effect on the cavity will likely allow us to improve the baseline optical loss and stability and thus the detection limits in the ICP-CRDS system. Very preliminary data suggests that improvement of the stability of ICP-CRDS may be possible through continuous wave ringdown techniques.

During the past quarter, laser-induced fluorescence experiments have been performed to test the performance of the modified dedicated ventline in order to insure that the vent exhaust does not disturb the ICP plasma, increasing measurement uncertainty. Our progress was slowed due to equipment difficulties related to two components of the LIF system.: a replacement unit for one of the components was received and successfully tested; the other component was repaired after extensive diagnosis.

**Laser-induced breakdown spectroscopy.** Efforts to improve the LIBS calibration for solid samples continued. In particular, the effect of varying the distance between the focusing lens and sample surface was investigated. The preliminary data demonstrate that a shorter lens to surface distance (LTSD) provides significantly better LIBS sensitivity and precision. More data were collected to determine the optimum LTSD for solid calibration. An optimum LTSD for LIBS calibration of solid sample was found to be -2.0 cm shorter than the focal length. LIBS calibration data of alloys were also collected using this optimum lens-to-surface distance.

---

### ***Environmental Control Device Testing***

**Performance enhancement of the ionizing wet scrubber.** DIAL currently is in possession of an ionizing wet scrubber (IWS) provided for testing by Ceilcote Inc. This scrubber is currently a part of the off-gas system at the TSCA-Oakridge incineration facility, and is under consideration for use in the DOE waste treatment processes. Current

plans are to primarily investigate the relationship of plate voltage with respect to particulate removal in this system. Since the system is a commercial scale system with high flow rates we had anticipated getting a loss of weight particulate feeder from the One Tenth Scale Combustion facility at the Savannah River Site and install it at our site. This would give us a particulate feed rate compatible to what is required for testing. The IWS has been set-up at the DIAL facility and we are still in the process of acquiring the particulate feed system.

**Testing of a ceramic regenerative heat storage device for dioxin control and heat recovery.** A novel regenerative heat recovery device promises to reduce dioxin emissions from incinerators, in addition to recovering waste heat for preheating the combustion air. Significant progress has been made during the last quarter--fabrication of the device is at least 50% complete and we are waiting for some other tests to be completed on DIAL's combustion test stand (CTS) before we can install and test the ceramic regenerator prototype.

**Transportable calibration test stand for diagnostic instrumentation.** A transportable calibration test stand is being developed for the purposes of construction of a test train that would be usable for calibration of optical diagnostic instrumentation. In this quarter we have developed a schematic and engineering drawings for construction of such a test stand. Currently we have put together a pre-heater and two mass flow controllers for air and propane injection into this two inch diameter combustion system. The dopant is being injected into the stream using a conventional nebulizer, although we will be trying an acoustic injection system. The DIAL-LIBS system is currently being used to measure metals concentrations in pre-heated air on this test bed. A burner has been designed and tested for use in this calibration stand. This same (propane/air) burner was used in the injection of metals solutions into the combustion test stream for testing of an ICP system being developed at Ames Lab.

**Evaluation and performance enhancement of a submerged bed scrubber.** This task is aimed at the evaluation and performance enhancement of a submerged bed scrubber for cleanup of effluent gas from low flow rate incinerations systems. We have completed the engineering drawings for the test system and are in the process of acquiring materials to assemble the test bed.

---

### ***Waste Treatment and D&D Support: Process Monitoring And Control***

**Dioxin and PCB Studies.** The formation of dioxins and furans during combustion processes has become a significant focus of concern over the past few years. EPA has initiated an intensive effort to characterize the different sources of dioxins in the US and to reduce the overall annual rates of emissions. The 1999 MACT for Hazardous Waste Combustors establishes an emission limit for dioxins and furans that will be technically difficult to achieve. Large strides to controlling dioxin and furan emissions from combustion processes will most easily come from an enhanced understanding of their mechanisms of formation. The work being conducted by DIAL will seek to reduce uncertainties associated with the locus of formation of these compounds and factors that contribute to their formation.

**On-line multi-spectral imaging of thermal treatment processes.** During the past quarter while waiting on delivery of components of the multi-species system, we explored the possibility of applying spectral imaging to long-term monitoring for DOE by recorded spectral images of cotton plant leaves grown under different conditions of nutrient stress. It is anticipated that by selecting appropriate spectral regions or ratios of spectral regions, it may be possible to discern the presence of heavy metal pollutants in plants. Significant progress in using neural networks was made this quarter; a program capable of discerning whether or not the species of interest is present in significant quantity is nearing completion.

**Imaging instrumentation application and development: thermal imaging.** To improve DIAL's thermal imaging system as to provide *in situ* monitoring of the thermal distribution inside the core chamber of treatment facility, the effects of the surface emissivity was studied. The software development of an user adjustable control for target surface emissivity was conducted. Search for an NIR camera started.

**Imaging instrumentation application and development: profilometry.** To improve the system flexibility in software development for imaging instrumentation, an integrated imaging acquisition software has been completed. To improve the system fringe pattern projection, a Xe strobe light projector has been integrated into the system to provide stronger light projection intensity. Further development of image analysis and result presentation is underway.

**Saltcake Dissolution.** ESP model predictions are compared with experimental results for the dissolution of a saltcake sample from Hanford tank 241-TX-113. Evaluation of the dissolution process for this particular saltcake has provided additional insight into the use of the ESP thermodynamic model at high sulfate concentrations. Inadequacies in the Public database have been observed at the high ionic strengths (~24) typically encountered at low diluent additions to the saltcake. Discrepancies in the model predictions resulted in the use of an additional database. This finding is of interest in the use of ESP by Hanford personnel in planning and staging retrieval operations. Comparison of the model predictions with the experimental data revealed that additional laboratory studies are needed on the sodium-sulfate-carbonate-hydroxide system. This later work will be pursued in FY01.

**Solids Formation.** Progress is reported on two tasks specifically designed to evaluate, predict, and consequently prevent solids formation associated with Hanford site operations. The unintentional formation of solids during waste transfers has lead to scheduling delays, increased operational costs, and large capital outlays. Delays in the

delivery of the waste during future vitrification operations can result in financial penalty.

The deposition of particles and the formation of plugs can result from unfavorable transfer conditions, such as low flow rates, line configurations with dead zones, and inadequate temperature controls, and from changes that may occur based on these parameters and the chemical composition of the fluid. Interactions between the operating conditions and the waste chemistry are complicated and the focus of the work. Results are presented for studies on salt well pumping and the development of an engineering tool that will allow site operators to tailor transfer conditions. The work is expected to result in the basis necessary to ensure the safe and efficient transfers of various waste streams at the site.

Details of the design, construction, testing, and evaluation of a laboratory-scale salt well pumping apparatus are given. The flow loop was developed to aid tank farm operators at Hanford by providing baseline data on supernate transfers from single-shell tanks. Work focussed on the use of a surrogate for Hanford tank 241-SX-104. Screening experiments were conducted in the laboratory and ESP calculations were performed. Experiments in the test loop revealed plug formation from trisodium phosphate dodecahydrate. This material has been observed to form long, rod-like crystals and will hydrate 12 moles of water for each mole of trisodium phosphate formed. ESP calculations predict a solids loading of 0.68% by weight at the gelation temperature and even at this concentration the rods form a sufficient number of secondary bonds to result in a three-dimensional structure.

Variations in pressures and temperatures were observed during plug formation. Experiments conducted at an initial Reynolds number  $R_{eD} = DV\rho/\mu = 223$  did not reveal a dependence of plug formation upon cooling rate owing to the efficiency of the heat exchanger. The heat exchanger was oversized and did not permit fine control of the

surrogate temperature at the low flow rate in the current configuration. Significant variations in the time needed to form a plug were found with an increase in  $R_{eD}$ . The average time needed to form a plug with the surrogate was 262 seconds at an  $R_{eD}$  of 223, 692 sec at  $R_{eD} = 319$  and increased to 2656 sec for  $R_{eD}$  of 436. Rapid plug formation was found at low stream velocities and a more gradual deposition was observed at the highest Reynolds number investigated. The change in deposition behavior and the phase change occurring in the solution at the gel point hinder the analysis of the data using conventional dimensionless numbers. Such an analysis is considered possible but additional data is required. Plans for future experiments are described.

Specifics of the modeling approach and the development phases of the engineering tool that will help prevent plug formation incidents during the Salt Well pumping and Slurry Transfer operations at Hanford are outlined. The efforts are mainly aimed at producing a model that will accurately predict, if, where and when a plug will form during a transfer process while taking into account the dynamic behavior of the transfer process and reflect the impact of the waste chemistry. Efficiency, ease of operator use, and applicability to the operations at Hanford are considered top priorities.

The modeling approach based on building the model using separate modules that represent a specific physical or chemical process, has started. A general Computational Fluid Dynamics (CFD) system that was capable of representing the transport module part was acquired. Initial test simulations for simple but relevant transport processes were performed. Other tests addressing module sensitivity to grid distribution, initial and boundary conditions, and initial velocity distribution at the entrance are in progress.

Simulations for the FIU Slurry C experiments which demonstrates the process of settling of a simple suspension produced good agreement with the reported results. The simulations suggested that

flow rates with entrance velocities larger than 1.0 meters/sec will produce a moving bed flow. The higher the flow rates the less likely a significant amount of particles will deposit eventually leading to the formation of a plug. To prevent the establishment of stationary bed flow, a pumping flow rate producing velocities higher than the settling velocity, for the largest particle available to transport, has to be used. This will insure a minimum of moving bed flow.

Incorporation of more elaborate formulation and additional modules into the overall model are in process. This will include capabilities that will account for the complex characteristics of the waste. Modifications will include the effects of the change of solids concentration on the viscosity of the flow, phase transition, particle nucleation and growth, and chemical reactions capabilities.

---

### ***Diagnostic Field Applications Coordination and Testing Support (DFACTS)***

**HEPA filter testing.** HEPA filters are used as the final air pollution control device before off-gases are released to the atmosphere. The required usage of HEPA filters is expected to increase in hazardous waste facilities as particulate emission standards become more stringent. There is growing interest in insuring that these filters are effectively used and properly monitored. The EPA is interested in data that will help in defining permitting conditions as well as in insuring that instrumentation and procedures for compliance assurance are available. At the present time there is no known particulate measurement system that is capable of monitoring HEPA performance. There is a current need to evaluate the potential of PM CEMs for use in HEPA filter performance monitoring or possibly as a “break through” detector. DIAL is working with the EPA DOE Technical Work Group for MOU Project on HEPA Filter Performance and Monitoring to start a

new project to evaluate the performance of HEPA filters under normal operating conditions.

## *Characterization of Heavy Metals, Radionuclides and Organics in Heterogeneous Media*

---

### ***Volatile Organic Compound Monitoring Using Diode Lasers***

*C. B. Winstead*

#### **Introduction**

The United States Department of Energy currently operates three mixed waste thermal treatment facilities (the TSCAI at Oak Ridge, WERF at INEL, and CIF at Savannah River). A concern for these and future DOE facilities is monitoring and controlling the release of volatile organic compounds in the facility off gas. For example, at least five needs are listed in the FY 2000 DOE Needs Database that directly request continuous emission monitors (CEMS) for species including organics. Of these five listed needs, four (SR00-1004, ID-2.1.18, ID-S.1.02, and ID-2.1.41) are rated as Priority 1 needs, implying that they are critical to the success of a given mission. The fifth (ID-3.2.32) is rated as Priority 2, indicating that a substantial benefit would be realized if the need were fulfilled. According to the Savannah River Site Need Statement (full text available at <http://www.srs.gov/general/srtech/stcg/Needs/sr-1004.htm>), for CEM purposes the desired detection limit for most organics other than dioxins is approximately 1 ug/m<sup>3</sup>. This corresponds in general to detection

limits in air just below the parts-per-billion range (e.g., 1  $\mu\text{g}/\text{m}^3$  of chlorobenzene or trichloroethane is approximately 0.2 ppb). In addition, solutions for numerous other organic monitoring applications are needed throughout the DOE complex (e.g. organic species in groundwater).

This project is a continuation of our previous work that focused on the evaluation of near-infrared diode laser spectroscopy for monitoring selected volatile organic compounds (VOCs) in air. That work utilized simple multipass absorption techniques to determine the effect of pressure broadening on the sensitivity of VOC detection at available diode laser wavelengths. Extrapolating from these experimental results for VOCs in air suggests that a technique known as diode laser cavity ringdown spectroscopy (DL-CRDS) could potentially achieve CEM level detection limits with no preconcentration. While our previous multipass absorption experiments indicated a detection limit of 20 ppm for benzene, DL-CRDS should be four to six orders of magnitude more sensitive. This level of detection is approximately equal to just slightly worse than the sensitivity required for an organic CEM. Therefore, an experimental evaluation of the achievable detection limits for VOCs using DL-CRDS is needed. The primary objective of this project is to construct a laboratory DL-CRDS system and determine its detection limits for selected VOCs. This information will be used to determine if a DL-CRDS system should be constructed for process gas monitoring next year.

The data gathered this year also will be used to guide the design and construction of an appropriate sampling interface for VOC measurements. Although it may be possible that a very advanced DL-CRDS system could achieve CEM detection limits directly in an off gas sample (pending the effects of pressure), for a robust industrial system it may be preferable to use preconcentration in a sampling system to reach lower detection limits. Preconcentration using adsorbent or cryotrap technology (e.g. a “purge and trap” method) is well developed for on-line gas chromatography (GC). The potential sensi-

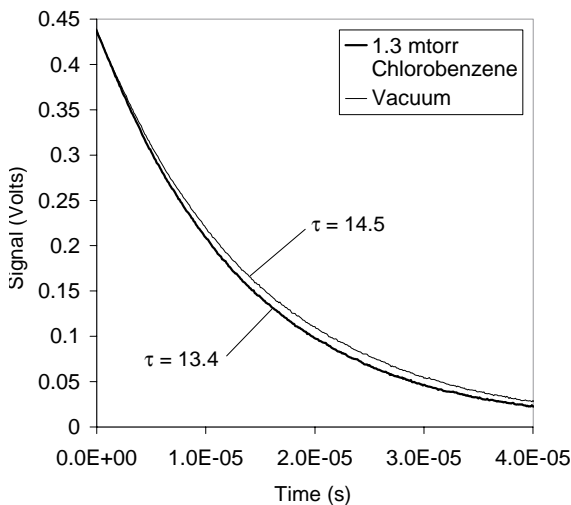
tivity of a DL-CRDS system should allow minimal preconcentration (10X - 50X) to be used, allowing for rapid measurements (e.g. every 15 minutes) without the operational complexity, maintenance, and calibration issues associated with GC. Thus, this year's laboratory measurements are essential to guide the design for the next year's sampling system. This work will also clarify our capabilities for meeting other DOE needs such as monitoring underground organic plumes, making perimeter or ambient air VOC measurements, or potentially monitoring particulate concentrations at very low levels.

### **Work Accomplished**

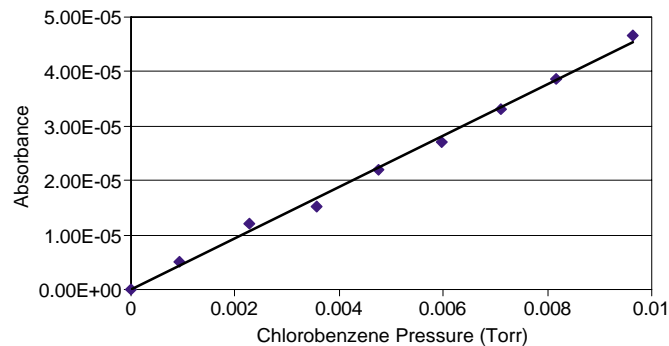
During this quarter, a gas handling system was constructed to allow the introduction of known quantities of VOC samples. This new sample introduction system was designed to allow the expansion of a high concentration of gas in a small volume into the larger volume of the measurement cell. The volume ratio of the two cells was used to calculate the concentration of analyte in the measurement cell to allow quantitative data acquisition with a known concentration of analyte. Measuring the higher pressure in a small cell greatly improves the accuracy of the sample introduction system, since the small pressures present in the measurement cell are difficult to measure.

Figure 1 depicts two ringdown curves obtained using the new system. These curves were acquired at a wavelength of approximately 1653 nm using a distributed feedback diode laser. A ringdown time of 14.5 microseconds is observed when the cell is evacuated. Upon introduction of a 1.3-mtorr chlorobenzene sample into the cell, the ringdown time drops to 13.4 microseconds as the laser light in the cavity is absorbed by the chlorobenzene. Figure 2 depicts a calibration curve obtained upon the introduction of several different pressures of chlorobenzene. As expected, a linear curve is obtained. Using the baseline noise level at the time of the measurement and the slope of the calibration graph, a detection limit of approximately  $1.5 \times 10^{-4}$

torr is obtained. This value corresponds to a detection limit of 200 ppb in air at atmospheric pressure. Future improvements to the system are expected to decrease this detection limit significantly.



**FIGURE 1. Comparison of ringdown waveforms with/without a VOC sample in the cell.**



**FIGURE 2. Calibration graph for chlorobenzene obtained with the DL-CRDS system.**

A presentation titled “Diode Laser Cavity Ringdown Spectroscopy for On-line Monitoring Applications” by C. B. Winstead, G. M. Molen, S. T. Scherer, A. C. Srivastava, and J. P. Singh was presented at the American Chemical Society’s 220th National Meeting in Washington, DC on August 20, 2000.

### **Work Planned**

A significantly lower baseline pressure is needed in the measurement cell to calibrate the system for lower detection levels. The current system is only evacuated by a roughing pump, and thus is only capable of pressures of approximately  $10^{-3}$  torr, nearly a full order of magnitude above the current estimated detection limit. During the next quarter, an improved vacuum system with a diffusion pump and cold head will be installed and used to reduce the baseline pressure of the system. This is expected to improve the reproducibility of the data obtained thus far, and allow measurements at even smaller VOC concentrations. While the system is envisioned to eventually operate at atmospheric pressure, this level of vacuum is required in order to mix calibration samples of such small partial pressure. Some improvements will also be made on the sample introduction system to allow for more rapid sample changes and improved reproducibility.

### **Nomenclature**

voc	volatile organic compound
CEM	continuous emission monitor
GC	gas chromatography
DL-CRDS	diode laser cavity ringdown spectroscopy

---

## *Sensitive Detection of Toxic Chlorinated Compounds*

*Ram Vasudev*

### **Introduction**

This project addresses the widespread need for a general-purpose, sensitive detector for toxic compounds, especially chlorinated organic compounds. Chemicals such as dioxins are among the most toxic man-made chemicals and are generated as unwanted by-products of incomplete combustion, metallurgy and during the manufacture of other chemicals. The need for their detection either directly, or through the detection of surrogates/precursors, has been a subject of intense research in many laboratories. Popular laser-based methods such as laser-induced fluorescence (LIF) and resonance-enhanced multiphoton ionization (REMPI), although quite sensitive in general, are susceptible to loss in sensitivity due to intersystem crossing (ISC) induced by the presence of chlorine. In addition, the loss in detection sensitivity is a monotonic function of the chlorine content, so for polychlorinated molecules the detection limits can be compromised. To circumvent this spectroscopic problem, we have been exploring a relatively new technique called cavity ring-down spectroscopy (CRDS). It is solely absorption-based and is thus not influenced by excited-state nonradiative decay, as shown by our work on chlorinated benzenes with varying chlorine content.<sup>1-3</sup> It is quite sensitive and, in principle, simple to implement, so it is a very promising *universal* toxic gas detector. We describe here our work towards developing a CRDS-based detector for dioxin-type molecules.

### ***Experimental Technique (Cavity Ring-Down Spectroscopy)***

As mentioned in our earlier reports, the high sensitivity of CRDS is due to the very long absorption pathlengths achieved by trapping a laser pulse between the mirrors of a high-finesse (low loss) optical

cavity. In suitable cases, the optical absorption pathlength can be several kilometers even though the cavity itself is considerably shorter ( $\leq 1$  m), so very small concentrations of chemical species can be detected.

The experimental setup has been described previously.<sup>1,2</sup> Briefly, tunable pulsed light from a frequency-doubled dye laser is injected into a confocal cavity containing an absorbing species. Light exiting the cavity decays exponentially on the microsecond time-scale and is monitored by a photodetector. The signal is captured by a transient digitizer and the decay constant (the “ring-down” time) is calculated as a function of the wavelength to generate the absorption spectrum.

## **Work Accomplished**

### *Dioxin Detection*

We had previously described the absorption spectrum of dibenzo-*p*-dioxin (DBPD) obtained by cavity ring-down spectroscopy.<sup>2,3</sup> We have now obtained a similar spectrum for 2-chloro-dibenzo-*p*-dioxin in the 260 - 310-nm region. As in the case of DBPD, the spectrum is quite extensive and is thought to be composed of two singlet←singlet electronic transitions.

### *Dioxin Precursors/Surrogates*

Work is continuing on this class of molecules. The emphasis is on detection limits and species-specificity. Our current detection limit is in the ppb range. Further improvements are possible.<sup>3</sup>

### *Data Acquisition Software*

Concurrent with the experimental work, we are developing real-time data acquisition software.

## Future Work

Work will continue on chlorinated dioxins and dioxin surrogates/precursors.

## References

1. R. Vasudev, in *Instrumentation Development, Measurement and Performance Evaluation of Environmental Technologies*. Technical Progress Report DIAL 40395-7, January - March 2000. Mississippi State University: Diagnostic Instrumentation and Analysis Laboratory.
2. R. Vasudev, in *Instrumentation Development, Measurement and Performance Evaluation of Environmental Technologies*. Technical Progress Report DIAL 40395-8, April - June 2000. Mississippi State University: Diagnostic Instrumentation and Analysis Laboratory.
3. I.V. Tretiakov and R. Vasudev, under preparation (to be published).

---

## *Isotopically Selective Monitors for Transuranic Elements*

*D. L. Monts and C. B. Winstead*

## Introduction

A number of DOE needs have been established that are related to the treatment or characterization of waste contaminated with uranium or transuranic (TRU) elements. For example, the Hanford site lists as needs the development of a technology for treating TRU waste contaminated with PCBs and ignitables (Need RL-MW06) and the development of a sensitive screening method for selected transuranic elements in soils in a near real time manner (Need RL-SS-14). Although these needs are very different in nature, each will no doubt require the development of a robust, yet sensitive detection system

capable of quantifying TRU element concentrations with isotopic resolution. Such a system would serve as a process monitor in one case and as an on-site analytical tool in another. In addition to needs listed in the DOE needs database, the Idaho National Engineering and Environmental Laboratory (INEEL) has expressed a need for monitoring residual TRU elements in treated high level waste. Specifically, a need exists for on-line monitoring of the low activity fraction of this treated waste after dissolution and partitioning. Such a system could replace expensive off-line sampling and analysis and eliminate the need for holding tanks in the Idaho HLW process. This project is primarily directed toward on-line monitoring application and thus is most relevant to the efforts of the High Level Waste Tank Remediation Focus area. However, future applications of the developed technology should make this effort relevant to additional needs in process control and on-site monitoring.

In spite of their radioactivity, detecting TRU elements at ultrasensitive levels has proven to be problematic for traditional radiological counting methods due to the very long half-lives of these predominantly alpha-emitting elements. A new approach is required to allow for rapid measurement of TRU elemental concentrations in an on-line or rapid on-site manner. Optical spectroscopic methods offer significant promise in such an application and are capable of reaching detection limits far below counting techniques in a very short measurement period. This proposal is concerned with the evaluation of two sensitive laser spectroscopic methods, laser-induced fluorescence (LIF) and cavity ringdown spectroscopy (CRDS), for potential use as TRU monitors. In laser-induced fluorescence, a laser is used to excite atoms of the selected element from one electronic state to another. The subsequent fluorescence emitted by the excited atom is monitored using a spectrometer and photomultiplier tube arrangement. Under appropriate conditions, the fluorescence intensity is directly proportional to the concentration of the element. In cavity ringdown spectroscopy, the time for a laser pulse to decay in an optical cavity is measured. Analyte atoms introduced into the cavity reduce this “ring-

down” time by absorbing light from the laser pulse. For both the LIF and CRDS efforts, atomic species will be generated by injecting standard or surrogate sample solutions into an inductively coupled plasma (ICP). The first step of both the LIF and CRDS processes is the same, namely absorption of laser photons by analyte atoms. The isotopic resolution of each technique is achieved in this first step by using a narrow linewidth laser to excite only one particular isotope of the element being measured. Although CRDS theoretically will detect all absorption events and thus might be expected to be the more sensitive of the two techniques, the simpler implementation and better signal-to-noise ratio of LIF could result in LIF being the preferred monitoring technique. Experimental evaluation of each technique is required. Recent regulatory approval for the use of uranium in our facility will allow this evaluation to proceed.

### *Purpose*

The primary purpose of this project is to evaluate LIF and CRDS for use as robust, isotopically selective, cost-effective, on-line TRU monitors for the INEEL high level waste processing facility. Knowledge of isotopic abundances is necessary since different isotopes can have widely differing activities. The niche for this technique is determination of concentrations and isotopic abundances for cases where current techniques are severely limited by low throughput, such as: (1) cases where the radioactivity is so low that radioactive decay disintegration counting techniques cannot analyze samples during acceptable counting periods; and (2) cases where lengthy sample preparation is required for mass spectrometric determination. The performance of these techniques will be evaluated using uranium standards and surrogate waste solutions provided by INEEL. The successful development and implementation of a TRU monitor could save millions of dollars through the elimination of holding tanks currently planned for the INEEL process. These tanks would be used to hold the treated waste prior to release while TRU analyses are performed on the tank contents. Clearly, this particular effort is most rel-

evant to the effort of the High level Waste Tank Remediation Focus Area. However, such a system could ultimately provide solutions for needs in other focus areas such as Mixed-Waste Characterization, Treatment, and Disposal. At the end of this project, a full analysis of the sensitivity and selectivity of LIF and CRDS for uranium monitoring will be reported, and recommendations for how to proceed in the construction of an isotopically selective, on-line TRU monitor will be presented.

### *Methodology*

**Cavity Ringdown Spectroscopy.** Cavity ringdown spectroscopy (CRDS) is an extremely sensitive variant of absorption spectroscopy that has been demonstrated in a variety of studies. Thus the ringdown technique will be only briefly summarized here. In the original form of CRDS, a laser pulse from a tunable pulsed laser is introduced into a stable optical cavity formed from two highly reflective mirrors (Fig. 3). A fraction of the laser pulse is injected through one cavity mirror and is trapped, propagating back and forth between the mirrors. A photomultiplier tube placed behind the second cavity mirror is used to monitor the time constant for the pulse to decay (also known as the “ringdown” time). The reflectivity of the mirrors and the absorption of a sample in the cavity determine the pulse decay time. The pulse interacts with an absorbing medium in the cavity over the course of potentially thousands of round trips, vastly increasing CRDS sensitivity over standard absorption methods. As the absorption in the cavity increases, the increased optical losses cause the decay time for the light in the cavity to decrease. By inserting into the cavity an appropriate atomization source, such as an inductively coupled plasma (ICP), very low concentrations of the various chemical forms of TRU elements can be atomized and detected by measuring changes in the cavity ringdown time constant.



**FIGURE 3. Schematic of cavity ringdown spectroscopy (CRDS) apparatus.**

**Laser-induced Fluorescence Spectrometry.** Laser-induced fluorescence (LIF) spectrometry is a well-established, robust technique for detecting species of interest at low concentrations. In the LIF technique (Fig. 4), an electronic state of the species of interest is excited with a tunable laser and the resulting fluorescence intensity is monitored as a function of laser wavelength. Since the mass of isotopes are different from one another, the corresponding atomic energy levels are slightly different (Fig. 5). Consequently, when a sufficiently high-resolution tunable laser is scanned across an atomic electronic transition, the resulting LIF spectrum contains a peak associated with each isotope present; the intensities of the isotopic peaks are directly related to the concentration of the isotope. Hence the isotopic abundances can readily be obtained from the LIF spectrum. In order that the individual isotopic transitions can be resolved, it is necessary that the species of interest be in the gas-phase. For the TRU elements of interest, an atomization source is required in order to volatilize and atomize the sample. A calibration curve is obtained by recording the LIF signal intensity as a function of concentration. Using the calibration curve, unknown concentrations can be determined.

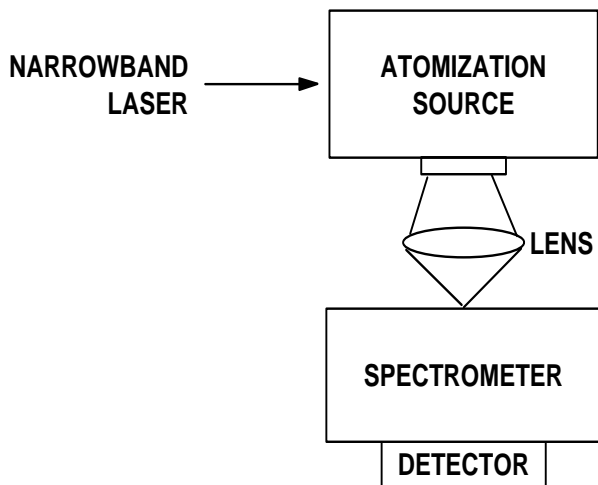


FIGURE 4. Schematic of the laser-induced fluorescence spectrometry technique.

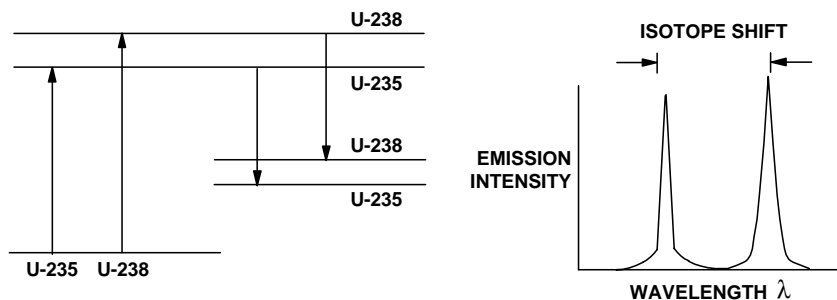


FIGURE 5. Schematic of isotopic energy shifts and the associated LIF spectrum.

## Work Accomplished

**Cavity Ringdown Spectroscopy.** Both the Nd:YAG and pulsed dye laser systems used for the CRDS experiments have been down for repair through most of this quarter. In the interim, we have carried out

numerous experiments investigating the effect of the ICP plasma on the mode structure in the cavity. An effect noticed very early in our ICP cavity ringdown work was that insertion of the plasma increased the background optical loss in the cavity and reduced the baseline stability of the ringdown time measurement. Understanding the physical mechanisms responsible for these effects may allow us to improve the performance of the ICP-CRDS system. This effort is being carried out using diode laser CRDS, providing additional experience using diode laser CRDS techniques with the ICP system. A future at-line or on-line TRU measurement system would likely be constructed in this fashion as opposed to the current laboratory system. Very preliminary data suggests that improvement of the stability of ICP-CRDS may be possible through these newer techniques. More will be reported on this as we achieve a better understanding of the underlying mechanisms at work in the interaction between the plasma and the cavity modes.

**Laser-induced Fluorescence Spectrometry.** The dedicated ventline in the LIF laboratory has been modified so that venting of the ICP head is better enclosed. A series of experiments have been begun to test the performance of this modification of the ventline.

In the past, the same laboratory room housed both the LIF project and the Spectral Imaging project. The LIF project is on the verge of beginning experiments with uranium which requires that the LIF laboratory be posted as a restricted area due to the presence of radioactive materials. In order to avoid exposing the Spectral Imaging personnel and equipment to the dangers and restrictions involved when radioactive materials are present, the Spectral Imaging project has been moved into available space elsewhere in DIAL, enabling final preparations for the radioactive work.

During this reporting period, our progress was slowed due to the equipment difficulties related to two components of the LIF system. A replacement unit for one of the components was received and suc-

cessfully tested. The other component was repaired after extensive diagnosis of the problem.

### **Work Planned**

**Cavity Ringdown Spectroscopy.** The Nd:YAG and dye lasers are each expected to be repaired within the next three weeks. As soon as possible, experiments for detecting and quantifying uranium in solution using ICP-CRDS will begin. The initial work will focus on the strong 386-nm uranium ion absorption line. Although this line does not possess an extremely large isotopic splitting, it should be resolvable with our current dye laser system. Following a determination of the uranium detection limit using this absorption line, we will likely investigate the absorption of the 424-nm ion line. This line is expected to be somewhat weaker than the 386-nm line, but has a very wide isotopic splitting.

**Laser-induced Fluorescence Spectrometry.** Early in the next quarter, we expect to begin experiments using uranium. Our efforts will concentrate on optimization of operating conditions for detection of uranium in an ICP plasma. Parameters to be optimized include carrier gas flow rate, position of the laser excitation beam within the plasma, choice of excitation and detection transitions. Since the CRDS group is also utilizing an ICP plasma source for their efforts and hence also needs to optimize their ICP plasma for uranium detection, the two groups will split the effort and share results; this will enable us to more extensively survey parameter space and to more quickly arrive at the optimum operating conditions.

A prerequisite for successful completion of this project is for a sufficiently narrow-linewidth, tunable laser system that can be reproducibly scanned. After optimization using naturally occurring uranium and our current dye laser, we, in collaboration with the CRDS group, will perform experiments using CRDS' moderately high-resolution dye laser system to evaluate whether or not that laser is suffi-

ciently narrow to isotopically resolve uranium. If as expected these LIF experiments prove that such a moderately high-resolution tunable laser system has sufficient resolution for uranium, then a comparable dye laser system will be purchased for this effort; if those experiments indicate that even higher resolution is required, then additional funding will be sought in order to purchase an ultra-high resolution tunable laser system.

### **Nomenclature**

CRDS	cavity ringdown spectroscopy
DIAL	Diagnostic Instrumentation and Analysis Laboratory
DOE	U.S. Department of Energy
HLW	high level waste
ICP	inductively coupled plasma
INEEL	Idaho National Engineering and Environmental Laboratory
LIF	laser-induced fluorescence
PCB	polychlorinated biphenyl
TRU	transuranic

---

## ***Laser-induced Breakdown Spectroscopy***

*C. F. Su, F. Y. Yueh and J. P. Singh*

### **Introduction**

This technical task has been focused on the development and application of laser-induced breakdown spectroscopy (LIBS) to monitor RCRA metals from thermal treatment processing facilities. LIBS is a laser-based, non-intrusive, and sensitive optical diagnostic tech-

nique for measuring the concentration of various atomic and molecular species in test media.<sup>4,5</sup> It uses a high power laser beam to produce a laser-induced plasma at the test point. The plasma atomizes and electronically excites the various atomic species present in the test volume in a single step. The intensities of the atomic emission lines observed in the LIBS spectrum are used to infer the concentration of the atomic species. LIBS has successfully demonstrated its real-time monitoring capability in various field tests.<sup>6-11</sup>

### **Work Performed**

Efforts to improve the LIBS calibration for solid samples continued. We investigated the effect of the distance between the focusing lens and sample surface on the LIBS signal. The preliminary data show that a shorter lens-to-surface distance (LTSD) provides significantly better LIBS sensitivity and precision. More data were collected in this work period to determine the optimum LTSD for solid calibration. Four samples (three glass samples and one aluminum alloy) were used in this study. In the experiments, LIBS signals were recorded with different LTSD with a lens of 30-cm focal length. Figure 6 shows the variation of the Fe 371.99-nm emission lines at different LTSDs from a glass sample. Experimental results of these samples unanimously indicated that the maximum spectral intensities were generated when the LTSD was less than the focal length, approximately between 1.5 and 2.5 cm. In the same region, the relative standard deviation of the average spectral intensity was also found to be the minimum.

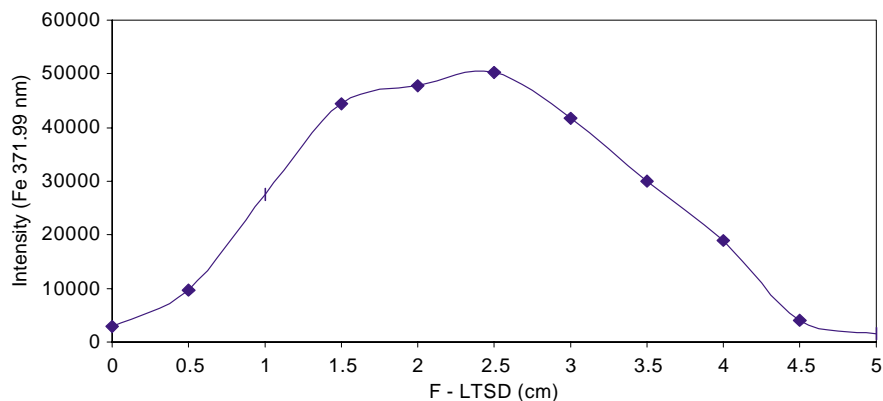


**FIGURE 6. LIBS signal obtained at different LTSD from a glass sample.**

---

We then recorded LIBS calibration data of aluminum alloys under the optimum experimental conditions. Eight Al alloy samples were used for this study. The concentrations of the major elements of each sample were analyzed by Mississippi State Chemical Laboratory with the atomic absorption spectroscopy technique. In principle, under the same experimental condition the LIBS spectral intensity of an element will only be dependent upon the concentration of the element present in the sample. Thus, the spectral intensity and the concentration should have a linear relation. The results of numerous experiments indicated that under certain conditions the spectral intensities of an element have a linear relation with the concentration of the element in the samples. These conditions are:

- the spectral lines with self-absorption cannot be used for analysis;
- the standard sample has to be homogeneous, due to the small sampling volume with LIBS;
- the spectral line used for analysis should be an interference-free line.

Figure 7 illustrates the relationship between the spectral intensities and the concentrations of Fe.

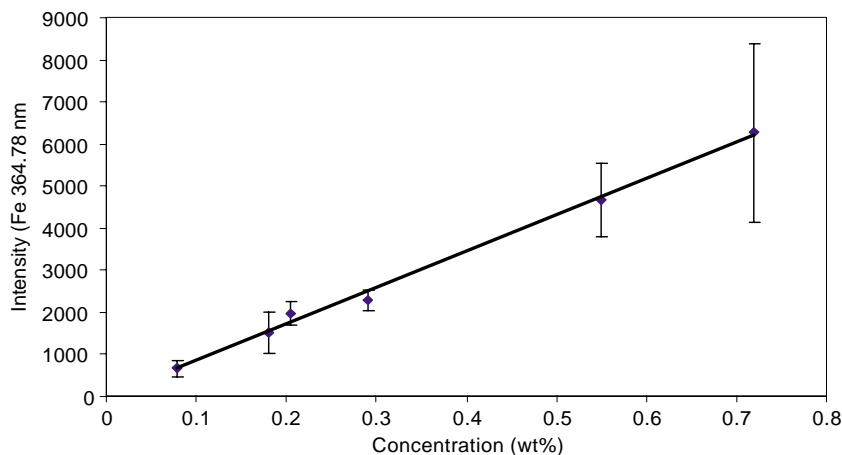


**FIGURE 7. Aluminum calibration for Fe.**

---

## Work Planned

Calibration data of glass and molten glass samples will be collected using the optimum experimental conditions. Study of liquid LIBS will begin. LIBS CEM tests will be conducted in the DIAL test stand.

## References

4. D.A. Cremers and L.J. Radziemski. 1987. Laser plasmas for chemical analysis. In *Laser Spectroscopy and its Application*, L.J. Radziemski, R.W. Solarz, J.A. Paisner, eds. New York: Marcel Dekker, Ch. 5, p. 351.
5. L.J. Radziemski and D.A. Cremers. 1989. Spectrochemical analysis using plasma excitation. In *Laser Induced Plasmas and Applications*, L.J. Radziemski and D.A. Cremers, eds. New York: Marcel Dekker, Ch. 7, pp. 295-326.

6. J.P. Singh, F.Y. Yueh, H. Zhang. 1997. *Process Control and Quality*, 10:247.
7. J.P. Singh, H. Zhang, F.Y. Yueh and K.P. Carney. 1996. *Applied Spectroscopy*, 50:764.
8. J.P. Singh, H. Zhang and F.Y. Yueh. February 1996. Transportable Vitrification System Shakedown Test, Westinghouse Savannah River Corporation and Diagnostic Instrumentation and Analysis Laboratory: Laser-induced Breakdown Spectroscopy Measurements. US DOE Contract No. DE-FG02-93CH-10575. DIAL 10575 Trip Report 96-1.3.
9. J.P. Singh, H. Zhang and F.Y. Yueh. April 1996. DOE and EPA Continuous Emission Monitoring Test at EPA National Risk Management Research Laboratory (NRMRL). US DOE Contract No. DE-FG02-93CH-10575. DIAL 10575 Trip Report 96-2.
10. J.P. Singh, H. Zhang and F.Y. Yueh. 1996. Plasma Arc Centrifugal Treatment PACT-6 Slip Stream Test Bed (SSTB) 100-hour Duration Controlled Emission Demonstration (CED) Test. DIAL Trip Report 96-3.
11. J.P. Singh, H. Zhang and F.Y. Yueh. September 1997. DOE and EPA Continuous Emission Monitoring Test at EPA National Risk Management Research Laboratory (NRMRL). DIAL Trip Report 97-1.

---

*Performance Enhancement of the Ionizing Wet Scrubber*

*R. ArunKumar*

**Introduction**

The IWS is one of the few commercial effective micron and sub-micron particulate removal system used to treat effluent gas from incineration and waste processing systems. The system operates essentially like a wet electro-static precipitator but there are some its theory of operation differs a little primarily with respect to the development of particulate charges. In this study we plan to enhance the performance of the IWS and overcome some of the problems associated with its operation. Current problems include plate life and performance with respect to plate spacing and applied voltage. Information obtained from this task should enable DOE operators of the IWS to operate more confidently this particulate cleaning device.

Baseline measurements of the IWS unit will initially be conducted in regards to its performance and particulate removal efficiency. In order to complete this task we will need a particulate feeder of a sufficiently large size to simulate particulate loading at the incinerator facilities. We hope to obtain the feeder that is currently at the

One-tenth Scale Combustion Facility at the Savannah River Site and install it at our site. We will survey the DOE incinerator sites and determine the order of importance of the operational issues that need to be addressed with the IWS. These may include some problems that we have not yet identified. We will then select the most important tasks that we think can be solved in the given time frame. As part of our technology transfer mission, and in exchange for lending the IWS unit to DIAL we will share the information gained with ITEQ the manufacturers of the unit.

### **Work Accomplished**

The IWS that has been installed at our site has been tested without any particulate feed.

We are still on hold with this project, awaiting the acquisition delivery and installation of the particulate feeder from the Savannah River site. The acquisition of the feeder is a specific go/no-go item under this task. We see the acquisition of the particulate feeder as a good addition to the facilities available at DIAL, because it will allow a lot of our instrumentation and DOE customer instrumentation to be tested under very realistic field conditions. With this in mind we are still pursuing the acquisition of the particulate feeder for this project, as well as for any future projects that may come our way.

### **Work Planned**

The primary task in the coming quarter still entails acquiring the particulate feeder. Once we take delivery of the system we will be able to install it on the IWS and commence testing.

---

*Testing of a Ceramic Regenerative Heat Storage Device  
for Dioxin Control and Heat Recovery*

*O. P. Norton*

**Introduction**

The new MACT standards for dioxins (0.2 ng/dscm TEQ) will challenge incinerator operators, the DOE included. DOE waste remediation facilities that will be impacted by these rules include the Consolidated Incineration Facility (CIF) at Savannah River and the TSCA incinerator at Oak Ridge. Also, we note that the processes that form dioxins and furans could also occur in other thermal waste treatment systems, such as vitrification systems and plasma torch-based systems, so the impact on DOE's EM program could be considerable.

Although our knowledge of dioxin formation mechanisms and kinetics is incomplete, it is generally accepted that dioxins and furans are formed as combustion products (flue gases with associated particulates and products of incomplete combustion) are cooled downstream of the combustor. Tuppurainen, et al.,<sup>12</sup> give the dioxin formation range as 250 to 650°C, with the maximum at about 300°C. Karasek and Dickson<sup>13</sup> found that the optimum temperature range for the formation of dioxins from pentachlorophenol was 250 to 350°C. Altwicker, et al.,<sup>14</sup> give the critical temperature range as 250 to 400°C. Although these different sources report slightly different critical temperature ranges for dioxin formation, it is fairly clear that dioxins and furans are formed at fairly low temperatures, as the combustion products cool.

This insight suggests that dioxin could be controlled by quenching--cooling the exhaust gases as quickly as possible through this critical temperature band. Rapid quenching is indeed a common

dioxin control mechanism in municipal solid waste incinerators, and dioxin formation can be minimized by this strategy.<sup>12</sup>

Santoleri and Budin<sup>15</sup> report: “Systems that are able to quench the high temperature combustion gases from 1000 - 1200°C to adiabatic (75 - 90°C) in fractions of a second have emissions well below the levels established by the MACT standards (0.2 ng/dscm TEQ).”

Thus, rapid quenching--cooling the flue gases through the critical temperature range as quickly as possible--is an effective method of dioxin control. Water sprays have been effective for dioxin control, but this method essentially wastes the thermal energy in the combustion products. Also, for hazardous and radioactive waste incineration, a secondary waste stream will be created.

We propose that a regenerative heat recovery system can be used to control dioxin emissions. Regenerators have long been used to recover waste heat from flue gases, using this heat to preheat the incoming combustion air. We observe that, if the cooling of the hot gases in the regenerator is sufficiently rapid, then dioxin formation should be minimized as well.

A novel regenerative heat storage device is proposed that can be used to suppress dioxin formation in the off-gas of a thermal waste treatment plant. The flue gas is rapidly cooled as it passes through the device to prevent the formation of dioxins and furans from the precursors that are present in the gas. When integrated into a waste incineration plant, this device can also be used to recover the sensible heat in the flue gas and provide preheated combustion air.

During the previous year, a computer model was developed for a pebble-bed regenerator, and this model was used to size a regenerator for DIAL's combustion test stand.

This computer model was used to size a pebble-bed regenerator for DIAL's combustion test stand. Our calculations indicate that this design will quickly cool the combustion products through the critical dioxin formation temperature range--with a mean residence time of 0.6 to 0.7 seconds. Thus, this regenerator design should provide effective dioxin control.

During the current year, we will build and test this device on DIAL's combustion test facility. With a newly designed and built piece of equipment, testing should proceed incrementally, at each step verifying that the equipment performs according to design. The test sequence will proceed as follows: First, cold flow tests will be performed with no combustion to verify that the flow switching valves work properly and that our control system is sequencing the valves properly. Then, hot testing will begin. These tests will be performed to verify the correct operation of the system, that the flow switching valves work at the high temperatures for which they were designed, and that the pebble beds cool the combustion gases as they should. During this phase of testing, the pebble beds will be instrumented with thermocouples to measure the inlet and outlet gas temperatures, as well as temperatures inside the pebble bed at selected locations. The flow rates of gases through the beds will be measured. Also, the pressure drop across each bed will be measured.

These results will verify proper operation of the regenerator. The temperature measurements will be compared to the predictions of our model, and we hope that this comparison will validate the model. Also, the temperature measurements will verify that the desired quenching rate has been achieved.

The ultimate objective of this test program will be to demonstrate that the degree of quenching produced by the pebble bed is effective in reducing dioxin emission. To do this, we would like to perform a series of tests on DIAL's combustion test stand, injecting dioxin precursors upstream, and measuring dioxin levels downstream.

We intend that the dioxin level downstream of the regenerator will be measured and compared to the control--the same test facility without the regenerator. We would, of course, take care that the combustion parameters, such as the fuel/air ratio, were the same in both cases. DIAL maintains an in-house capability to perform dioxin measurements using EPA Method 23.

However, we must point out that there is currently some uncertainty about our permitting to carry out tests of this nature. Once this situation is resolved, then a detailed test plan for the dioxin testing will be written before the start of these tests, and submitted to the Task Monitor for approval.

After the computer model has been validated by experiment, and we have verified that the rate of quenching is effective in reducing dioxin emissions, the validated computer model will be used to assess various approaches to scaling up. Maximum pebble bed size will be determined. Multiple regenerator configurations will also be studied as a possible approach to large scale operation.

### **Work Accomplished**

Fabrication work has begun and is at least 50% complete. Some delay has been encountered due to scheduling conflicts on DIAL's Combustion Test Stand (CTS).

### **Work Planned**

The prototype will be installed in the CTS and tested, as outlined in the introduction.

## References

12. K. Tuppurainen, et al. 1998. Formation of PCDDs and PCDFs in municipal waste incineration and its inhibition mechanisms: a review. *Chemosphere* 36:7:1493-1511.
13. F.W. Karasek and L.C. Dickson. 1987. Model studies of polychlorinated dibenzo-*p*-dioxin formation during municipal refuse incineration. *Science* 237:754-756.
14. E.R. Altwicker, et al. 1990. Polychlorinated dioxin/furan formation in incinerators. *Hazardous Waste and Hazardous Materials* 7:1.
15. J.J. Santoleri and M.L. Budin. May 1998. *The impact of thermal oxidation quench systems on dioxin formation*. IT3 Conference: International Conference on Incineration and Thermal Treatment Technologies, Salt Lake City, Utah.

---

## ***TranSportable Calibration Test Stand for Diagnostic Instrumentation***

*R. ArunKumar*

## Introduction

With the advent of modern diagnostic techniques for Continuous Emission Monitors (CEM) and Process Monitors (PM), a need has evolved for the development of a bench-scale test train, which can be used for process simulation as well as for calibration of such instrumentation. The application of some of these instruments is limited by the availability of calibration streams, especially for low concentrations. In this task we aim to construct a versatile test bed that will be able to provide a test bed for calibration of optical diagnostic instrumentation over a range of temperature of temperature and concentration levels, for both combustion and non-combustion applications.

The system as shown in Figure 8 comprises of an air flow, fuel flow, and dopant delivery streams. The air delivery system contains a pressure regulator, followed by a thermal mass flow measurement and control system, and an electric air heater. A dopant solution is delivered to a nebulizer or acoustic atomizer, which injects it as a fine mist of droplets into the throat of a venturi in the air delivery system. Propane is regulated, and its flow is controlled by a similar thermal mass flow meter/controller and injected into the throat of a second venturi in the air delivery system. The throat of a venturi provides a convenient place for injection of secondary streams, providing a lower pressure and also a smaller cross-section for more uniform dispersion. This combustible air stream is then ignited using a spark plug in the burner. The burner itself consists of a short water-cooled section followed by a hotter un-cooled tube to maintain flame stability.

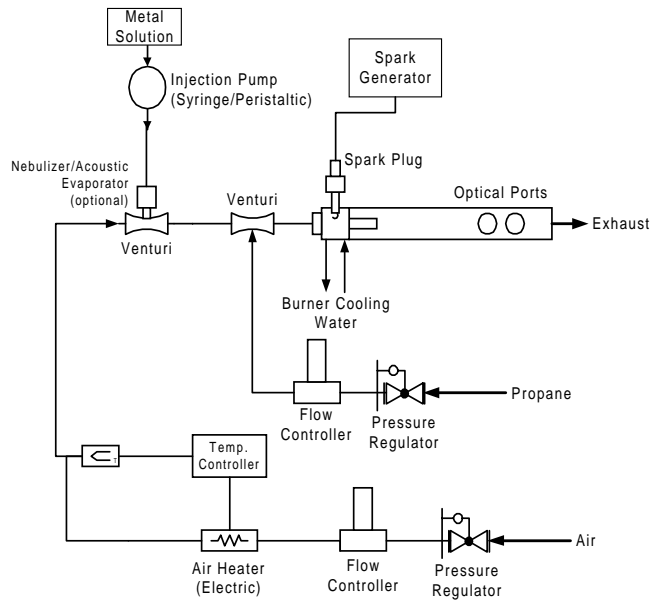


**FIGURE 8. Schematic of the transportable calibration test stand for diagnostic instrumentation.**

## Work Accomplished

The system has now been put together and is in operation. LIBS measurements on pre-heated air are still undergoing. The combustion and burner part of the system were used for injection of heavy metals solutions into the DIAL combustion test stand. These runs on the combustion test bed were for the testing of an on-line ICP system being developed by Ames Lab. Heavy metals solutions were injected into the inlet air to the propane-fired burner in a venturi section upstream of the burner. It was expected that the RCRA metals (initially in a nitrate form) in the solutions would oxidize on going through the combustion process. The doped burner exhaust gases emptied directly into the combustion test stand gas stream, on top of a measurement section, to provide a well-metered concentration of the dopants. The combustion performance of the burner was very successful, with a stable flame and steady gas temperatures in the test section. There is, however, some doubt about the performance of the acoustic atomization system that was initially used to inject the heavy metals solution into the burner stream. This was based on measurements made by the Iowa State APOGEM-ICP system. A nebulizer was then used successfully for the injection of the metals solutions into the burner air stream. Initial examination of the test results appear to conclude that measurements were as expected, based on solute and gas stream concentrations. We will concentrate on refining the acoustic atomization system used for the burner in the coming quarter. Along with this, LIBS measurements on the combustion stream will be continuing.

---

## *Evaluation and Performance Enhancement of a Submerged Bed Scrubber*

*R. ArunKumar*

### **Introduction**

Submerged bed scrubbers (SBS) were originally developed by PNNL for treatment of off gas from nuclear reactors. SBSs have been proposed for use on the cleanup systems for scrubbing off-gases from liquid-fed ceramic melters used to vitrify high level waste, and from other thermal processes. SBSs serve dual purposes in that they act as a quench for high temperature exhaust gas and also remove at least 90% of the airborne particulate matter. These scrubbers are however susceptible to certain kinds of problems including poor gas distribution, gas surging, channeling and bumping. In this task we propose to add a better gas distribution system under the SBS as well as replace the conventional spherical bed media with an engineered aggregate produced by Ushers, Inc. This “tetrajack” material more efficiently fills the bed volume than spheres (> 90% fill), and forces the gas stream to follow a tortuous path through the SBS.

Figure 9 shows a scale model of the West Valley SBS that has been constructed. It is primarily split into two parts i.e the gas distribution section and the scrubber bed section. Constructed of clear acrylic the dual section assembly will allow us to observe, as well as readily test different configurations of the gas distribution system.

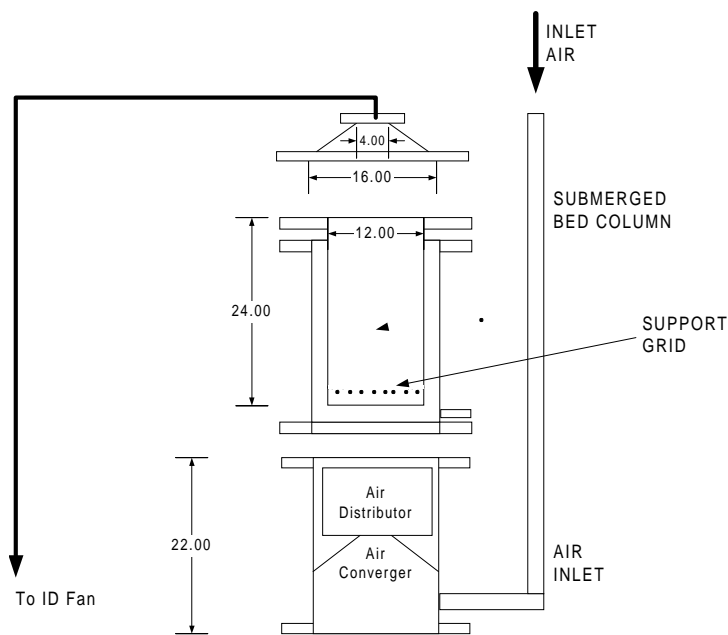


**FIGURE 9. Scale model of West Valley submerged bed scrubber.**

Operation of the test bed without modification will first be performed to develop baseline performance data. The gas distribution in the bed will be observed visually, as will gas surging through the system. If needed, a positive air pressure delivery system can also be used to study gas distribution. Flow stability and surge parameters can be detected using differential pressure sensors. The first aspect of the testing will be to ensure that a uniform distribution of the gas is obtained under the submerged bed using a positive pressure feed system. This will be followed by testing using an induced draft fan, where surge effects can be determined and minimized. EPA measurements to determine particulate retention will be completed in the final stage of the testing. Capture of fine particulate material (talc or titania particles) and of simulated semi-volatile material (Cs salt) will be monitored, as will SBS operating parameters (e.g., flow rate, pressure drop).

At this point, the system will be cleaned, and the spherical bed material will be replaced by Ushers proprietary material. The baseline testing will be repeated to evaluate the performance of this material. Then, the SBS model will be disassembled, and a flow distribution system will be inserted and tested with conventional (spherical) bed material. The same parameters will be monitored and evaluated.

### **Work Accomplished**

The test bed has been completed and preliminary testing is beginning to determine air flow rates. The system is ready to be used with both forced air from the DIAL test facility as well as induced air using an ID fan at the exit of the system.

### **Work Planned**

The next quarter will be devoted to devise an effective air distribution system under the submerged bed scrubber. Tests with both conventional glass marbles and the tetrajack material should then also be underway.

## *Waste Treatment and D&D Support: Process Monitoring and Control*

---

### *Dioxin and PCB Studies*

*C. Waggoner*

#### **Introduction**

Selected congeners of the families of dioxins and furans (D/F) are potentially some of the most carcinogenic compounds known to exist. Recognition of the potential risk to the U.S. population spurred the conduction of a national inventory of D/F sources. A significant outcome of this initiative has been the establishment of a strategy to reduce emissions in a targeted fashion. One of the centerpieces of the D/F reduction strategy is the Maximum Achievable Control Technology (MACT) standard just issued for hazardous waste combustors (HWC). Each of the DOE hazardous or mixed waste incinerators falls subject to this new standard and there are stringent emission levels that will need to be met in the near future.

The 0.2 ng/dsm<sup>3</sup> emission standard called for under the HWC-MACT stresses the technical limits of operational control and emissions testing. Uncertainties associated with US EPA reference method stack sampling accuracy and method quantification limits for the 17 D/F congeners that have non-zero toxicity equivalence factors

invite skeptical review of the measurements that will be made by facilities to demonstrate compliance with this new standard.

Of the six needs listed on the DOE EM-Needs web page related to dioxin/furan problems, three (ID-3.2.32, ID-S.1.02, and SR00-1021) recognize the lack of knowledge associated with the specific locus of D/F formation, the distribution of D/F congeners between adsorbed and gaseous phases at temperature, and/or the behavior of these classes of compounds in the sampling train. This lack of knowledge is an impediment to minimizing emissions by process control or design/operation of pollution control devices. Additionally, a much fuller understanding of the phase behavior in off-gases is essential to development of a functional continuous emission monitor or verifying the accuracy of extractive sampling methodologies. Finally, a clearer picture of the gas phase chemistry is the best hope of identifying a dependable analytical surrogate, if one exists.

Intensive research has been undertaken throughout the past two decades to gain a more complete understanding of the mechanism(s) of dioxin/furan formation in combustion processes. The majority of controlled mechanistic studies of D/F formation tend to be carried out using bench top and micro-scale apparatus. A significant body of data has also been accumulated from off-gas samples collected from solid waste incinerators and industrial processes. However, the large number of variables associated with fuel feed and operational history of incinerators makes it difficult to extrapolate from bench to full scale. A series of studies is proposed to take advantage of bench scale results and, in a two-stage manner, extend these investigations to pilot scale.

The primary focus of this effort will be to determine the behavior of D/Fs associated with fly ash particulates in an isothermal off-gas environment for the temperature range of 300 to 800 F. This will include analysis of samples for D/F homologies to determine the

extent of formation, destruction, and dechlorination under test conditions.

All of the results from these investigations will be utilized, along with literature information, in the initial development and evaluation of a hybrid artificial intelligence system (combination neural network-expert system) to project D/F formation, identify areas of needed research, and search for analytical surrogates.

### **Work Accomplished**

During the second quarter of this fiscal year our efforts have been directed toward: (1) fabrication of the small-scale test stand; (2) fabrication of the isokinetic and isothermal sampling system; (3) continuation of development of the database of literature values for D/F distribution in the solid and vapor phases as a function of temperature; (4) continuation of AI software development; and (5) working with other EPA and DOE funded researchers to coordinate DIAL efforts with their research activities.

Fabrication of the combustor, flight tube, and flight tube housing have been completed. A prototype particle feeder has been developed and the next generation unit is under fabrication. Assembly of the different elements of the system has been completed in the high bay area of DIAL. Initial testing of the combustor has been completed however, problems have been encountered with condensation of water of combustion in lower portions of the flight tube assembly. Modifications are currently under way to increase temperatures in the flight tube to the 300 to 800 F range called for in the test plan.

The particle impactor has been fabricated and is ready to be used with the small-scale test stand. Problems were encountered in locating crushable metal seals that would not be considered catalytic to formation of D/Fs during the sampling process. Due to the temperature profiles called for in our test plan, steps would need to be taken

to preclude galling of threads in an impactor that is assembled from threaded sections. Anti-galling pastes or sealing were found to contain volatile compounds that would serve as a source of aromatic hydrocarbons and/or chlorine. After extensive searching, a source of reasonably priced crushable stainless steel seals has been identified the impactor was fabricated for assembly using bolts and these seals.

The Dioxin 2000 Conference in Monterrey, California was attended and numerous researchers consulted regarding attributes of the test apparatus and test plan for this research effort. Additionally, discussions were held with Drs. Barry Dellinger of LSU and Bryan Gullett of USEPA. Both are planning trips to DIAL to become more familiar with our capabilities and continue discussions on how DIAL can better coordinate our D/F research efforts with those of these established leaders. Some adjustments have been made to the test plan for this year's effort as a result of these discussions.

Selection of parameters to be used in formulation of an AI software package is continuing. Data reported in the proceedings of the Dioxin 2000 Conference are being incorporated into this database.

### **Work Planned**

During the next quarter, the small scale test stand will be modified by addition of heating tape for preheating the unit and adding thermal input required to achieve the desired operating range for the reaction flight tube. A more durable version of the low flow particle feeder will be fabricated and calibrated. The complete ensemble of test stand elements will be assembled and the unit characterized with regard to variation of temperatures in the isothermal flight tube section, particle flow rates, and off-gas chemistry. The modified impactor-based off gas sampling train will then be evaluated with regard to particle loading capacity and particle removal efficiency.

## References

16. K.L. Froese and O. Hutzinger. 1997. *Environmental Science and Technology* 31:542-547.
17. A. Addink, H.A.J. Govers and K. Olie. 1998. *Environmental Science and Technology* 32:1888-93.
18. P.M. Lemieux and J.V. Ryan. 1998. *Waste Management* 18:361-370.
19. P.H. Taylor and B.J. Dellinger. 1999. *Anal. Appl. Pyrolysis* 49:9-29.
20. F. Iino, T. Imagawa, M. Takeuchi, and M. Sadakata. 1999. *Environmental Science and Technology* 33:1038-43.

---

## *On-line Multi-Spectral Imaging of Thermal Treatment Processes*

*D. L. Monts and Yi Su*

### Introduction

Many of the DOE waste streams, particularly those currently stored in steel barrels, are poorly characterized or even uncharacterized. Given the variety of contents that can dramatically vary from barrel to barrel, it is necessary for thermal treatment systems (TTS) to quickly change operating parameters and/or implement divert-and-treat measures when specific species of environmental concern (such as mercury) are suddenly introduced into the TTS. It is desirable to monitor species of concern inside the primary TTS chamber in order to provide the maximum possible response time and because concentrations will be higher here and hence easier to detect.

Digital images contain a wealth of information that if extracted, could be of immense value for monitoring/controlling a process.

Imaging spectroscopy combines conventional imaging, spectroscopy, and radiometry technologies to produce images for which a spectral signature is associated with each spatial resolution element (pixel). The emphasis of this project is on extending previous work to include extraction of information on concentrations, concentration distributions, and other parameters of use for process control of thermal treatment systems of interest to DOE. Using visualization and neural network techniques, the information can be presented in such a manner as to assist decision-making. Extraction of information from the primary thermal treatment chamber will provide sufficient time for operational parameters to be changed to maintain optimum operational performance and/or to allow divert-and-treat actions to be taken for species of environmental concern. Previous work at DIAL has shown utility of digital images for visual display of thermal distribution contours and for determination of average temperatures.

### ***Methodology***

Combining spectral and spatial analyses allows application of imaging technology to species characterization and detection inside primary chambers of thermal treatment sources for mixed hazardous waste processing. We are developing a spectral imaging system by combining a charge-coupled device (CCD) camera with narrowband optical filters. For the proof-of-concept experiments, a series of narrowband interference filters are utilized to obtain images of the combustion chamber at wavelengths characteristic of selected metal species. Subsequent efforts will employ an acousto-optic tunable filter (AOTF) in order to significantly increase the number of different wavelengths (and hence species) that can be monitored by the imaging system. The digital images are analyzed using commercially available software that is being modified to meet the needs of this project. We are also developing the methodology to calibrate the spectral imaging system. Analysis of the spectral images will be combined with neural network techniques in order to provide facility

operators with practical information on a time-scale short enough to enable process control decisions to be made.

### **Work Accomplished**

Previously we assembled a prototype spectral imaging system by using narrow band interference filters with CCD cameras and successfully demonstrated proof-of-concept for application of spectral imaging to quantitative detection of metal species in a practical thermal treatment system. After completion of the proof-of-concept experiments, we began working toward our next milestone, which is purchasing essential equipment and assembling the imaging spectrometry system for multi-species detection. A new dedicated data acquisition and analysis computer was ordered and received; the high processing speed of the computer facilitates rapid analysis of the spectral images. The ultraviolet acousto-optic tunable filter (UV AOTF) was ordered during March with delivery expected in July; delivery has been delayed because the manufacturer is experiencing technical difficulty providing the specified system. Progress on the “hardware” portion of our development effort is dependent upon receipt of the UV AOTF unit.

While waiting on delivery of the UV AOTF system, a five-filter filter wheel was ordered and received; this enables us to record sequential spectral images in five different spectral regions. To explore the possibility of applying spectral imaging to long-term monitoring for DOE, we recorded spectral images of cotton plant leaves, provided by other researchers at MSU. The cotton plants have been grown under different conditions of nutrient stress. Figure 10 shows spectral images of the same cotton leaf recorded using four different spectral regions. We have found that cotton plant stress due to nutrient deficiency can be ascertained from spectral images before it is visible to the eye, and that ratios of spectral images can be used as indicators of particular stresses: the ratio of the 700-nm and 800-nm spectral images (or the 700-nm and the 760-nm spectral images)



Our efforts to further refine and improve our data analysis computer subroutines continued. Our neural network efforts are currently directed toward determination of the concentration of a single species in near real-time from spectral images of thermal treatment. Significant progress in using neural networks was made this quarter; a program capable of discerning whether or not the species of interest is present in significant quantity is nearing completion.

### **Work Planned**

When the UV AOTF arrives, we will assemble the multi-species system and begin optimization of the system. We will begin the next round of DIAL test stand experiments, employing several species. Selection of species is based on (1) the presence of strong, spectrally isolated emission in regions of high detection sensitivity and (2) the ability to obtain permission to introduce the selected species into the DIAL test stand at concentrations that will not interfere with simultaneous or subsequent experiments performed by other DIAL research teams. Species currently under consideration for the next round of DIAL test stand experiments include (but are not limited to) Li, Mn, and Co. Work on the spectral imaging of plants will proceed on a time available basis.

### **Acronyms**

AOTF	acousto-optic tunable filter
CCD	charge-coupled device
DIAL	Diagnostic Instrumentation and Analysis Laboratory
DOE	U.S. Department of Energy
TTS	thermal treatment systems
UV	ultraviolet

---

## ***On-line Monitor for Gall Layer Detection***

*Gene Ramsey*

### **Introduction**

Work has been performed to design, test and develop a monitor for detecting the presence of sulfate salts (gall) on the surface of a glassy melt. This project is intended to deliver an on-line prototype for use with waste vitrification systems.

The second work period has been primarily devoted to the design, construction and installation of a high temperature furnace for the glass/gall experiments. The furnace design was based on the results of the room temperature experiments. The crucible can be viewed from a range (approximately 45°) of angles, thereby allowing definite experiments to be performed for determining the optimal orientation of the camera above the melt surface.

The furnace has been completed and installed and crucibles and materials for the initial thermal experiments have been acquired.

### **Work Accomplished**

Furnace designed with shortened crucible to camera length – mimics angles of orientation above common glass furnaces.

Furnace constructed with variable top arrangements for rapid change-out.

All installation activities complete – calibration begun (completed late November).

DOE glass process frit with low sulfate solubility acquired for realistic glass/gall testing.

### **Work Planned**

As described in the last quarterly, the furnace was in operation within six weeks of parts delivery. Delivery was seven weeks behind desired schedule due to furnace design requirements.

---

## ***Imaging Instrumentation Application and Development: Thermal Imaging***

*Ping-Rey Jang*

### **Introduction**

DIAL's thermal imaging system has been successfully used to monitor thermal distribution on various types of waste treatment furnaces. The viscosity of the melt and volatility of species in the melt are functions of the temperature and composition of the melt. Thus, it is essential to measure the melt temperature during the treatment process. It is also critical that the facility operator be able to view the surface of the melt bath from the temperature distribution point of view so that appropriate on-line process control/adjustment procedures can be justified.

Temperature measurement is based on Planck's radiation law assuming a gray body radiator. An ideal radiator, called a blackbody, will have a hemispherical spectral emissive power given by Planck's law,

$$e_B(\lambda, T) = \frac{C_1 \lambda^{-5}}{[\exp(C_2/\lambda T)^{-1}]}, \quad (\text{EQ 1})$$

where  $e_B$  is the emissive power,  $\lambda$  is the wavelength,  $T$  is the absolute temperature of the blackbody,  $C_1$  and  $C_2$  are constants. Temperature is determined by measuring the spectral emittance of a blackbody at any wavelength. In reality, most radiators are not blackbodies and so have a lower emissive power at the same temperature. The ratio for the spectral emissive power of an object to that of a blackbody at the same temperature is the object's emissivity,  $\epsilon_\lambda$ . The spectral emissivity, which may have values between zero and one, will depend upon the object's physical properties and may be a function of wavelength. The spectral emissive power of any radiator is given by

$$e_B(\lambda, T) = \frac{\epsilon_\lambda C_1 \lambda^{-5}}{[\exp(C_2/\lambda T)^{-1}]}. \quad (\text{EQ 2})$$

### **Work Performed**

The system development objective of this technical task during this period is to enhance the image system software with an adjustable emissivity plug-in value. With the emissivity value obtained from DIAL's Two-Color Pyrometer (TCP) system, the accuracy of the temperature within a target surface can be greatly improved. Software modules for the emissivity adjustment have been completed. The integration of these modules with the thermal imaging system software is completed. The final validation tests of the system with a standard temperature calibration source will follow. To improve the current system's temperature measurement range and increase its sensitivity, a search for a NIR camera began. Several manufacturers have been contacted for specifications and pricing. Research on a market available sensor within the allocated budget continued.

## Work Planned

Work will continue on the final validation tests with a standard temperature calibration source for the thermal imaging system. The search for a NIR camera to expand the sensor spectral response region into the near infrared will continue. The required system software development will follow.

## Reference

21. P-R. Jang, R.D. Benton and R.L. Cook. June 1994. *Some observations on the spectral response in pyrometry*. AIAA 94-2445.

---

## ***Imaging Instrumentation Application and Development: Profilometry***

### Introduction

DIAL's profilometry system was developed to measure surface profiles before and after a surface has been changed or scabbed. By utilizing Fourier transform profilometry (FTP), an imaging process technique, the volume and depth of material removed from the surface can be calculated.

The technique for the decontamination and decommissioning (D&D) of concrete structures within the Department of Energy and the nuclear industry is to remove a specific amount of material from the surface using a technique known as scabbling. The profilometry system developed at DIAL utilizes a structured light pattern projected onto a surface, and by analyzing the distortions of the pattern using a digital camera, the shapes of the object can be determined. As a wall removal monitor, the technique uses a projected light pattern that is cast onto the surface of the wall. An image is captured before work is

started on the surface, and a second image is captured after the work has been completed. Processing the two images yields the new surface profile relative to the original surface. Volume and depth of material removed from the surface can be calculated. The development of this system addresses DOE-EM and nuclear industry needs in the decontamination and decommissioning (D&D) of concrete structures.

### **Work Performed**

An integrated imaging acquisition software program was completed. Software modules for the image data file process, the strobe light-camera synchronization, and the image frame grabbing acquisition/display were completed. Also completed were the system integration tests for this newly developed imaging acquisition system. Images were acquired with the established components synchronization. A validation feature was also provided for the on-line histogram analysis of the user interactively selected region of interest (ROI) within the acquired image. This ensures the quality of the target image while the operator fine tunes the camera system. A graphical user interface was developed that not only initiates grabbing the target image frames but also provides the housekeeping modules for saving acquired images into the disk accordingly.

As the result of the intensity comparison of the sun light and the Xe strobe light, blockage of direct sun light interference was necessary to achieve proper projection of the Ronchi ruling. For the measurement environment where there was no direct sun light on the target area, the Xe strobe light projector provided a strong uniform fringe pattern which is vital to the success of FTP image analysis.

## Work Planned

Work will continue on the software development for the imaging analysis in the new ANSI C-based development platform. To improve the image resolution, system development for a high resolution digital camera will begin.

## Reference

22. M.E. Henderson and R.D. Costley. June 1998. *Wall removal monitor*. DIAL Technical Memo FTP 698.

---

## *Saltcake Dissolution*

*R. K Toghiani, J. S. Lindner, and H. Al Habbash*

## Introduction

This project is a continuation of the work previously reported on the dissolution of Hanford waste saltcakes. A main portion of the work is to continually validate and upgrade a thermodynamic equilibrium model, the Environmental Simulation Program (ESP) as applied to the Hanford wastes. Toward this end a number of significant accomplishments have been reported previously.<sup>23-27</sup> These include the evaluation of the code for the dissolution of saltcakes varying in composition through a comparison of model predictions with experimental results on core samples performed at the site, the use of the model to aid in the development of remediation strategies for Hanford tank 241-SY-101, an evaluation of data preprocessing, and the experimental determination of the solubility of natrophosphate, a double salt observed in the tank wastes.

A main focus is in bolstering the predictions of the code through comparison with experimental data and with other thermodynamic models such as SOLGASMIX. Accurate data called by the model are an essential requirement for quantitative code predictions; however, it must be noted that evaluation of the thermodynamic interactions between all of the species existing in the waste streams is not possible. The path, therefore, has been to concentrate on those anions such as nitrate, nitrite, hydroxide, sulfate, phosphate, fluoride, oxalate, carbonate, and cations, sodium, aluminum, calcium, nickel, uranium, etc., and the associated solids from these species that comprise the majority of the waste composition. Once assured that the code predictions accurately reflect the thermodynamics of these systems, it becomes possible to further upgrade the model to include other species of considerably lower concentration. The project is divided into three Tasks as summarized below.

***Task 1. Comparison of ESP to other thermodynamic equilibrium codes***

The model has been shown to provide agreement with literature data for the solid liquid equilibrium behavior of many of the saltcake constituents at both high and low ionic strengths. Nonetheless questions will remain on the application of the model to situations where the ionic strength is high owing to the extrapolation of fundamental electrolyte theory to regions of high ionic strength. Theoretical calculations for the most prevalent solid in the waste, sodium nitrate, will be performed at high ionic strength and compared to an alternate model developed by M. Ally at ORNL. Comparisons with the SOLGASMIX model, in collaboration with C. F. Weber (ORNL) will be performed for the sodium-fluoride-sulfate system. Companion solubility experiments will be made on this system to improve the ESP database (Task3).

***Task 2. Comparison of ESP predictions to saltcake dissolution experiments***

Previous work has characterized saltcakes with roughly four typical compositions as anticipated in the Hanford tank wastes. These

studies have indicated that ESP can be used to predict the dissolution behavior of the majority of the solids present. An exhaustive search for other types of saltcake compositions was conducted recently by D. L. Herting of NHC resulting in the identification of two additional tanks with different composition distributions. A sample from tank TX-113 will be evaluated this year. In addition, recent interest in pre-treatment and retrieval operations has indicated that there may be some concern when supernates from different waste streams are combined. ESP will be used with the predicted supernates from some of the previous saltcake dissolution studies to examine the propensity of solids formation under expected operating conditions. Predictions will be compared with on-going experimental work at the site.

A conference on the dissolution of saltcake will be organized and this forum will provide for extended discussions on the progress and results of the work and on future programmatic directions. Reports on the saltcake dissolution studies and on the outcomes of the saltcake dissolution conference will be provided.

*Task 3. Improvements and user documentation for the ESP model*

Some deficiencies have been shown to exist within the ESP data-banks.<sup>23</sup> Of high interest is the determination of solubility data for double salts. Solubility studies for  $\text{Na}_3\text{FSO}_4$  will be conducted and compared to the results of the prior literature and the calculations performed in Task 1. Additional studies on the extent of hydration as a function of ionic strength will be performed for  $\text{Na}_2\text{CO}_3$  and  $\text{Na}_3\text{PO}_4$ .<sup>28</sup> Experiments are also planned for NaF at elevated ionic strength and in the presence of  $\text{NaNO}_3$ .

Considerable effort has been expended in learning the most appropriate ways in which to develop and run ESP simulations. These will be documented and forwarded to customers at Hanford for incorporation in the ESP User Manual.

## Work Accomplished

### *Results and Discussion*

#### *Saltcake compositions*

The saltcake chosen for examination during FY00 was from tank TX-113. This saltcake contains significant amounts of a number of anions and was chosen to examine the predictive capabilities of ESP when a variety of species are expected to be present in the solid phase. The saltcake composition, determined from total sequential dissolution experiments conducted by Herting is shown in Table 1 along with the compositions of the four saltcakes examined during FY 98 and FY 99.<sup>29</sup> The compositions of the saltcakes studied in prior years are included for comparison.

**TABLE 1. Major constituents in saltcakes examined (weight percent of sample).<sup>a</sup>**

	<b>TX-113</b>	<b>BY-102</b>	<b>BY-106</b>	<b>A-101</b>	<b>S-102</b>
H <sub>2</sub> O	12.90	26.51	14.7	31.2	(5.0)
Al <sup>+3</sup>	0.32	1.65	1.58	2.39	0.67
Ca <sup>+2</sup>	0.02	0.043	0.013	0.008	
Cr <sup>+3</sup>	0.04	0.199	0.113	0.17	0.12
Fe <sup>+3</sup>	0.03	0.053	0.019	0.014	(0.03)
K <sup>+</sup>	0.03		0.243	0.31	0.07
Mn <sup>+2</sup>		0.024			
Na <sup>+</sup>	30.55	27.75	24.98	21.20	23.0
Ni <sup>+2</sup>		0.026	0.006		
P		0.998	0.078	0.14	0.18
Si	0.04	0.072	0.017	0.027	0.03
S		2.03	0.447	0.8	0.13
U	0.15	0.064	0.019	0.034	

**TABLE 1. Major constituents in saltcakes examined (weight percent of sample).<sup>a</sup>**

TIC <sup>*</sup>	15.07 <sup>b</sup>	4.13	1.43	1.81	0.59
C <sub>2</sub> O <sub>4</sub> <sup>-2</sup>	0.04	1.99	1.26	1.35	0.17
Cl <sup>-1</sup>	0.06	0.11	0.16	0.41	0.16
F <sup>-1</sup>	0.60 <sup>c</sup>	1.17	0.62	0.069	<0.02
NO <sub>2</sub> <sup>-1</sup>	0.26	1.85	2.71	7.43	2.04
NO <sub>3</sub> <sup>-1</sup>	19.12	10.92	40.54	12.6	53.7
OH <sup>-1</sup>	0.30	1.09	1.14	2.1	0.42
PO <sub>4</sub> <sup>-3</sup>	3.75	(0.06)	0.34	0.44	0.56
SO <sub>4</sub> <sup>-2</sup>	16.67	5.12	1.16	2.41	0.38
TOC		0.63	0.48	0.56	0.17
<sup>a</sup> Data from references <sup>26,29</sup> ; ( ) represents questionable result <sup>b</sup> Reported as CO <sub>3</sub> <sup>2-</sup> <sup>c</sup> Estimated result <sup>*</sup> Total inorganic carbon (CO <sub>3</sub> <sup>2-/5</sup> )					

As evidenced by the data in Table 1, the TX-113 saltcake contains the largest weight percentages (of any of the saltcakes examined thus far) of sodium, carbonate, phosphate, and sulfate, with the sulfate weight percent being significantly higher than in other saltcakes. Examination of a saltcake such as this provides the means to probe the predictive capabilities of ESP with respect to certain species. In this case, the predominance of sulfate in the original saltcake provides the mechanism through which deficiencies in ESP's representation of the various sulfate-containing solid species can be identified. The saltcake from tank BY-102, which contained significantly more carbonate than the other samples examined during earlier work, allowed deficiencies in ESP, with respect to sodium carbonate monohydrate and sodium carbonate decahydrate speciation under high ionic strength conditions, to be identified.<sup>24</sup>

*Data pre-processing for low-water content saltcakes*

In the FY 99 status report<sup>24</sup>, a recommended method for data pre-processing was detailed. This approach combined charge reconciliation by proration coupled with an iterative scheme to adjust the estimated input density to water analyzer to provide a weight percent water in the equilibrated stream equivalent to that measured experimentally by Herting. This approach was successful in generating ESP molecular streams that had the appropriate loading of the various anions and cations for three of the saltcakes examined during earlier work (BY-102, BY-106, and A-101). These saltcakes all contained a significant amount of water. For the remaining saltcake, S-102, it was not possible to adjust the estimated input density low enough to provide the experimentally determined weight percent water without encountering convergence problems within the water analyzer component of ESP. The saltcake from S-102 was reported by Herting to be extremely dry (no readily identifiable liquid phase at 0% dilution). The saltcake from TX-113 was similar in its physical constitution (very dry, no identifiable liquid phase). Strategies for ESP simulation of saltcakes with low water content are important so that the ESP simulation package can be routinely applied during operations planning at the Hanford site.

In order to avoid data pre-processing problems with the TX-113 input stream, similar to those encountered during FY 99 with the S-102 saltcake, sufficient water was added to the original saltcake composition prior to data input to the water analyzer. For a basis of 100 g of saltcake with the composition given in Table 1, 20 g of water were added to the mixture and ppm (mg/kg) values were calculated. Concentrations were then computed using an arbitrary density value. Addition of water in this manner does not alter the adjustment of cations and anions during charge reconciliation. However, it does impact the molalities for the various species into which the cations and anions are partitioned by the water analyzer component. The impact of water addition is mitigated during the iterative step in the recom-

mended method for data pre-processing where the estimated input density (input as an entry in water analyzer) is adjusted to achieve the experimentally measured percent water by weight. For treatment of low water content saltcakes, however, this is the step that gave rise to convergence difficulties. Rather than trying to match the experimentally determined percent water by weight of the original saltcake by adjusting the input density, the estimated input density was adjusted using the concentration of nitrate anion in the solution at a dilution of 300% by weight. For all of the saltcakes examined during FY 98 and FY 99, sodium nitrate, if present in the original saltcake, was completely dissolved at this level of diluent addition. Nitrate was also a significant component in all of the saltcakes examined and concentrations realized for nitrate anion were well above the limit of detection by ion chromatography.

A basis of 1200 kg of saltcake was used as input to the ESP program. This represented the 1000 kg of original saltcake equilibrated with diluent at a 20% addition level (200 kg diluent). To achieve a level of 300% diluent addition, 2800 g of water were added to the 1200 kg of saltcake using the MIX block available in ESP. The equilibrated output stream was examined to make sure that all the nitrate was partitioned into the liquid phase and the nitrate concentration was computed. This calculated concentration was then compared to the experimentally measured nitrate concentration reported by Herting for a dilution level of 300%. The estimated input density to water analyzer was adjusted in an iterative manner until the calculated nitrate concentration was approximately equivalent to the experimentally measured nitrate concentration at a dilution level of 300%.

In the FY 99 status report<sup>24</sup>, ESP predictions of the series dissolution test performed by Herting for S-102 were reported. These predictions used the molecular stream generated using the recommended reconciliation and density tuning approach.<sup>24</sup> A systematic deviation between experimentally measured nitrate concentration and that pre-

dicted by ESP was evident in the comparison plot, reproduced as Figure 30.

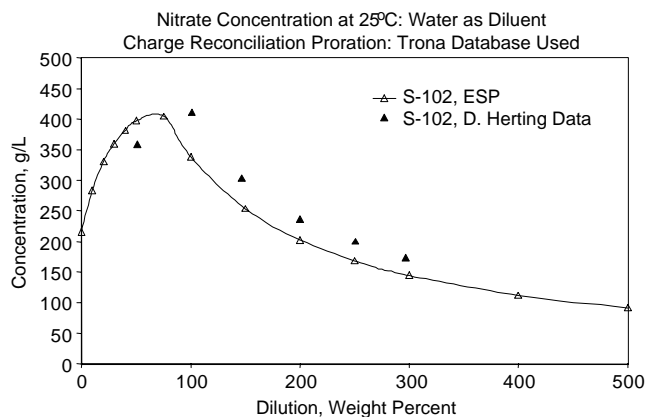


**FIGURE 12. Prior (FY 99) comparison of predicted and experimental nitrate anion concentrations for Tank S-102.**

The predicted concentrations are all lower than the experimentally measured values reflecting the fact that the input molecular stream generated for S-102 contained more water (~16%) than the original saltcake sample (experimentally reported value ~5%). In an effort to correct this systematic error in prediction, the strategy employed for charge reconciliation and density tuning for TX-113 saltcake was also applied to S-102 saltcake.

The molecular streams generated for both TX-113 saltcake (including the 20% dilution water) and S-102 saltcake (including 30% dilution water) are listed in Table 2. These molecular streams

were used for input to the ESP simulation program for the series dissolution modeling predictions.

**TABLE 2. Molecular streams for TX-113 and S-102 saltcakes generated using revised strategy for pre-processing of low water content saltcakes (units are molality).**

Species	TX-113 <sup>a</sup>	S-102 <sup>b</sup>
H <sub>2</sub> O	55.5087	55.5087
Al(OH) <sub>3</sub>	0.521157	3.05693
Ca(OH) <sub>2</sub>	0.021929	
Cr(OH) <sub>3</sub>	0.033805	0.290647
Fe(OH) <sub>3</sub>	0.023605	
H <sub>2</sub> CO <sub>3</sub>	7.10591	
HCl	0.145991	0.526999
H <sub>6</sub> F <sub>6</sub>	0.073169	
HNO <sub>2</sub>	0.244337	5.0344
HNO <sub>3</sub>	13.3315	98.2247
KOH	0.033717	0.216171
Na <sub>6</sub> (SO <sub>4</sub> ) <sub>2</sub> CO <sub>3</sub>	3.75134	
Na <sub>7</sub> F(PO <sub>4</sub> ) <sub>2</sub> ·19H <sub>2</sub> O	0.85356	
NaOH	29.9097	111.969
H <sub>2</sub> C <sub>2</sub> O <sub>4</sub>	0.019647	0.620668
NaPHOH		0.620668
Na3HSO42		0.189093
Trona		2.78316
<sup>a</sup> incorporates 20 g water per 100 g original TX-113 saltcake <sup>b</sup> incorporates 30 g water per 100 g original S-102 saltcake		

### *Simulation of saltcake dissolution experiments*

The ESP process model for this experiment consisted of three unit operations: a MIX block, a HEATER block, and a SEPARATE block. In the MIX block, the molecular stream describing the overall saltcake composition for a particular tank and including the water of dilution (added during the molecular stream generation described earlier for low-water content saltcakes) is combined with the required amount of diluent to achieve the desired level of dilution. For TX-113, a basis of 120 kg of saltcake (100 kg saltcake plus the 20 kg dilution water) is input as one stream. Additional diluent water is added through a second stream. Equilibration of the 120 kg saltcake stream provides the predictions used to determine solid/liquid phase partitioning at a 20% level of dilution. To achieve a 50% level of dilution, the 120 kg of saltcake would be combined with 30 kg of additional diluent water (50% dilution by weight of the original saltcake). Equilibration in the MIX block is achieved at 1 atm and 25°C. The equilibrated stream from the MIX block is passed to a HEATER block, where the temperature of the outlet stream leaving the HEATER block is adjusted to the laboratory equilibration temperature (either 25°C or 50°C). The effluent from the HEATER block is then passed to a SEPARATE block where the stream is partitioned into the relevant (solid and liquid) phases.

Preliminary ESP simulations were conducted using version 6.3 along with the PUBLIC database and the Trona (TV60TRON) database. The Trona database was incorporated as a result of FY99 work that indicated that the PUBLIC database was incapable of properly representing the behavior of sodium carbonate species (monohydrate and decahydrate) under high ionic strength conditions. Incorporation of the Trona database was found to significantly improve the predictions for carbonate and nitrate anions in the liquid phase as well as sodium carbonate monohydrate in the solid phase.

Series dissolution experiments were simulated over the range of xx% to 500% by weight addition of water (xx indicating the percent water which had to be added to the original saltcake in order to generate a molecular stream in the Water Analyzer component; e.g., for TX-113, the range examined was 20% to 500%). As detailed in the FY99 report, the anion concentrations reported from the ESP predictions were obtained by summing weighted contributions from all aqueous species containing a particular anion.<sup>26</sup>

**Thermodynamic database selection.** Initial simulations for the TX-113 saltcake, conducted using the Public database and the Trona database, indicated the need for improved thermodynamic data for the sulfate species; in particular, sodium sulfate anhydrous, sodium sulfate decahydrate, and the sodium fluoride sulfate double salt. In Figure 30, predictions for sulfate anion are shown along with the experimental measurements from the series dissolution tests of Herting for TX-113 saltcake.<sup>29</sup> The calculated ionic strength at a dilution level of 50% is ~ 24.4. The sulfate concentration predictions exhibit behavior typical of a species that is entirely found in the supernate, while the experimental data exhibit behavior typical of a species undergoing dissolution as diluent is added. This behavior is very similar to that exhibited by the carbonate anion in preliminary simulations for the BY-102 saltcake.<sup>26</sup> The preliminary simulations with BY-102 saltcake led to the decision to incorporate the Trona database in order to adequately describe the carbonate behavior under the high ionic strength conditions present in the Hanford saltcake waste. Discussions with OLI personnel identified a similar database for anhydrous sodium sulfate ( $\text{Na}_2\text{SO}_4$ ) and sodium sulfate decahydrate ( $\text{Na}_2\text{SO}_4 \cdot 10\text{H}_2\text{O}$ ). This database, Na2snacl, had been developed by OLI personnel to address the behavior of the sodium sulfate system under high ionic strength conditions.

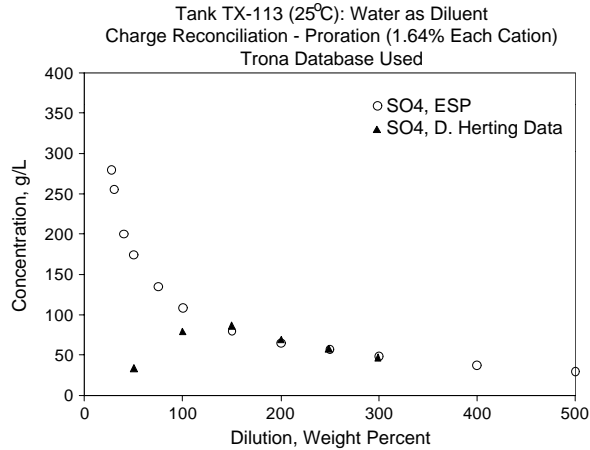


**FIGURE 13. Comparison of ESP prediction and experimental data for sulfate anion from series dissolution tests on TX-113 saltcake, 25°C**

Incorporation of this database with the Public and Trona databases significantly improved the predictive capabilities of ESP with respect to sulfate anion in the TX-113 saltcake. Figure 30 provides a comparison of the sulfate anion experimental data and the predicted values obtained when the Public, Trona, and Na<sub>2</sub>snac1 databases are used. The high percentage of sulfate in the original TX-113 saltcake was important in identifying the need for this specialized database. All ESP simulations discussed in this status report were carried out using Version 6.3 of ESP and the combination of three databases: Public, Trona, and Na<sub>2</sub>snac1.

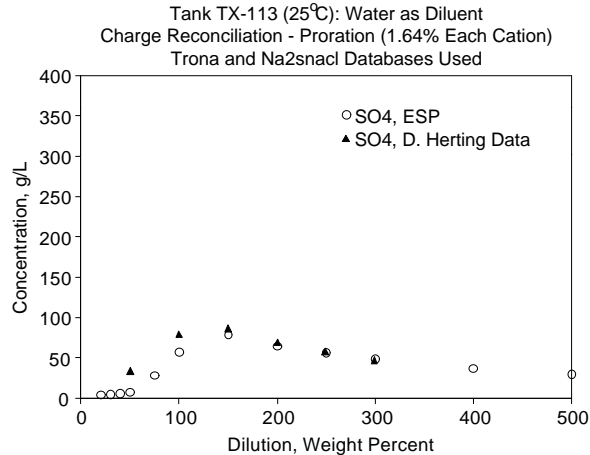


**FIGURE 14. Comparison of ESP prediction and experimental data for sulfate anion series dissolution tests on TX-113 saltcake, 25°C, incorporation of Na<sub>2</sub>SO<sub>4</sub> database.**

Comparison of model calculations with experimental results for nitrate, carbonate, and sulfate for TX-113 saltcake. The TX-113 saltcake contains significantly more sulfate by weight than the other saltcakes examined through Herting's dissolution studies. Nitrate, sulfate and carbonate account for approximately 50% by weight of the saltcake, with sodium accounting for another 30% by weight. Although the weight percent of phosphate in this saltcake is low compared to the weight percent of other components in the saltcake, the level of phosphate in the TX-113 saltcake is also approximately six times greater than phosphate levels in the saltcakes examined earlier. The level of carbonate in the TX-113 saltcake is comparable to that present in the saltcake from tank BY-102. The combination of these various anions in greater amounts provides a means to validate ESP when the saltcake is relative free of liquid (similar to the S-102 saltcake) and contains significant amounts of certain anions that have been identified with formation of various double salts. Herting identified the nitrate-sulfate double salt ( $\text{NaNO}_3 \cdot \text{Na}_2\text{SO}_4 \cdot 2\text{H}_2\text{O}$ ) as the major component in the solid phase of TX-113 saltcake.<sup>29</sup> As ESP does not have thermo-

dynamic data available for this species, its presence as a solid cannot be predicted by the ESP code. However, comparison of ESP predictions for the sodium-nitrate-sulfate system as a function of ionic strength and of temperature with SOLGASMIX predictions and literature data indicate that the lack of thermodynamic data for the double salt within ESP does not significantly impact the prediction of the solubility envelope.<sup>30</sup>

Figure 15 provides a comparison of the nitrate concentrations experimentally determined by Herting with the ESP predictions at various levels of diluent addition at 25°C. Nitrate, accounting for 20-weight percent of the original saltcake, is predicted to partition into the solid phase up to 30% diluent addition. Above this level of diluent addition, the nitrate concentration exhibits behavior indicative of a dilution process and is entirely found in the liquid phase. At a 50% diluent addition, the ESP prediction for the nitrate concentration is approximately 250 g/L, while the experimental data point is approximately 20% higher, 300 g/L. This may, in part, be due to the incomplete thermodynamic data for the sodium-nitrate-sulfate system as contained in ESP. Since the sodium-sulfate-nitrate double salt includes two moles of hydration water per mole of nitrate, the failure of ESP to predict this double salt could lead to the lower nitrate concentrations obtained by ESP. At the lowest level of diluent addition (20%), the solid phase is predicted to contain approximately 213 grams of anhydrous sodium sulfate (~1.5 gmol) and approximately 103 grams of sodium nitrate (~1.2 gmol). If the entire nitrate was present as the double salt, this would require ~ 2.4 gmol of water (waters of hydration).

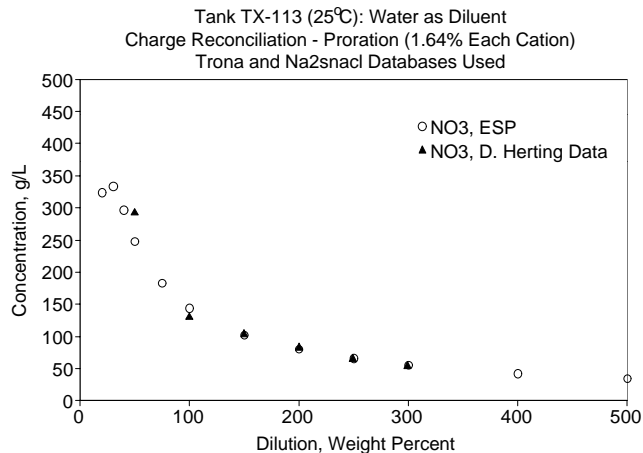


**FIGURE 15. ESP predictions and experimental nitrate concentrations for TX-113 Saltcake at 25°C.**

As a result, concentrations in the supernate would increase by approximately 10%. The discrepancies between predictions and experimental data in the low dilutions region are most likely due to the absence of thermodynamic data for the sodium-sulfate-nitrate double salt as well as deficiencies in the thermodynamic data for the other double salts, sodium-fluoride-sulfate and sodium-fluoride-phosphate. These deficiencies have previously been identified as the major contributor to differences between ESP predictions and experimental data from the dissolution tests in this region of low diluent addition (0 to 100%). Figure 16 provides the same comparison between ESP predictions and experimental data at 50°C. Again, no noticeable discrepancies are present except in the region of low diluent addition. SOLGASMIX predictions for the sodium-sulfate-nitrate double salt undertaken by Weber indicate that at this temperature, the double salt is not predicted to form.<sup>30</sup> Thus, the discrepancies between the ESP predictions for nitrate concentrations and the experimental measurements of Herting for TX-113 saltcake in the region of low diluent addition are attributed to deficiencies in ESP's ability to represent the

behavior of other double salts of interest, including the sodium-carbonate-sulfate double salt at this higher temperature.

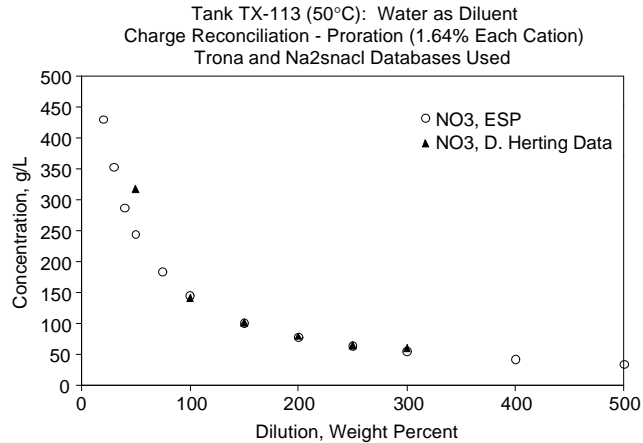


**FIGURE 16. ESP predictions and experimental nitrate concentrations for TX-113 saltcake at 50°C.**

Experimental and predicted TIC concentrations at 25°C are shown in Figure 17 for the TX-113 saltcake. Although the model results for dilution levels of greater than 100% agree quite well with the experimental data, ESP overestimates the concentration of TIC in solution at dilution levels of less than 100% by weight. A maximum in the TIC concentration is predicted at approximately a 50% by weight dilution, with a magnitude of ~36 g/L, while the experimental value is ~12 g/L. ESP predicts a significant fraction (~1/3) of the solid phase will be the sodium carbonate monohydrate salt and that the remainder of the TIC is partitioned into the liquid phase. At 50°C, the carbonate is partitioned into the solid phase as the sodium-sulfate-carbonate double salt, Na<sub>6</sub>(SO<sub>4</sub>)<sub>2</sub>CO<sub>3</sub>, rather than as sodium carbonate monohydrate. In contrast to the predictions at 25°C, the carbonate concentrations demonstrate better agreement with the experimental data as shown in Figure 18. In the solid phase, the sodium-sulfate-carbonate double salt is predicted to contribute ~ 53% of the solids at

the lowest level of dilution (20% by weight), increasing to ~91% of the solids before finally going into solution at dilutions greater than 200% by weight.

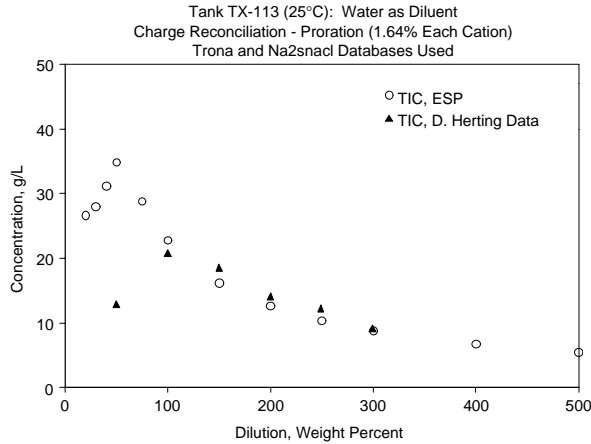


**FIGURE 17. ESP predictions and experimental TIC concentrations for TX-113 saltcake at 25°C.**

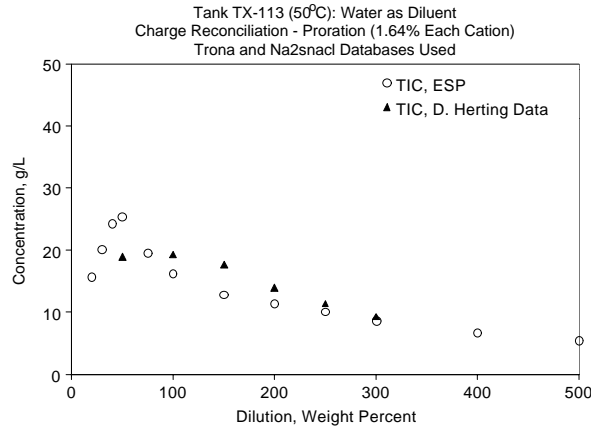


**FIGURE 18. ESP predictions and experimental TIC concentrations for TX-113 saltcake at 50°C.**

As demonstrated in Figure 13, use of the Public database alone will not provide for adequate representation of the behavior of sodium sulfate under high ionic strength conditions. Model predictions for sulfate concentration for the series dissolution of the TX-113 saltcake sample was previously given in Figure 14. While the representation at dilution levels of greater than 200% are in agreement with the experimental measurements, ESP predictions for the lower region of dilution (up to 150% diluent addition by weight) are lower than the experimentally measured concentrations. This implies that ESP is predicting more sulfate to partition into the solid phase than is present experimentally. At 20% diluent addition, the major constituents of the solid phase predicted by ESP include anhydrous sodium sulfate (~32% by weight), sodium carbonate monohydrate (~30% by weight), the sodium fluoride-phosphate double salt and sodium nitrate; with these species accounting for over 95% of the solid phase by weight. Only a small fraction of the solid phase is in the form of the sodium-fluoride-sulfate double salt (~3% by weight of the solids at 20% diluent addition). The combination of overestimation of carbonate concentrations with underestimation of sulfate concentrations in the region of lower diluent addition prompts one to consider the sodium-sulfate-carbonate system and whether the formation of the sodium-carbonate-sulfate double salt is impacted by the high ionic strength conditions present in the saltcake at these lower levels of dilution. Due to the thermodynamic data present in the Public database, this double salt is not predicted to form at 25°C, but can form in the temperature range 30°C to 150°C.

A preliminary attempt to identify the source of the combined differences in sulfate and carbonate concentrations at 25°C was made by exporting the thermodynamic data for the sodium-sulfate-carbonate double salt to a private database. The lower temperature limit of 30°C was modified and replaced with a lower temperature limit of 25°C. Saltcake dissolution at 40% diluent addition was simulated using this modified database for the sodium-sulfate-carbonate double salt and the solids phase distribution changed markedly with respect to car-

bonate and sulfate partitioning in the solid phase. Table 3 provides the solid phase distribution for the base case simulation of 40% diluent addition, with and without inclusion of the sodium-sulfate-carbonate double salt as a potential species in the solid phase. The solid species distribution changes little, except for the speciation of the sulfate and carbonate in the solid phase. The carbonate partitioned into the solid phase for either case can be evaluated using the molecular weight of carbonate per mole of the solid species into which it is partitioned. For the base case, this results in

$$\begin{aligned} \text{kg}(\text{CO}_3) &= \frac{177.83 \cdot (12.011 + 3 \cdot 15.9994)}{(2 \cdot 22.9898 + 12.011 + 3 \cdot 15.9994 + 2 \cdot 1.00797 + 15.9994)} & \text{(EQ 3)} \\ &= 86.1 \text{ kg}(\text{CO}_3) \end{aligned}$$

When the special database including the sodium-sulfate-carbonate double salt is used, the carbonate partitioned into the solid phase is:

$$\begin{aligned} \text{kg}(\text{CO}_3) &= \frac{335.57 \cdot (12.011 + 3 \cdot 15.9994)}{(6 \cdot 22.9898 + 2 \cdot (32.064 + 4 \cdot 15.9994) + 12.011 + 3 \cdot 15.9994)} & \text{(EQ 4)} \\ &= 51.6 \text{ kg}(\text{CO}_3) \end{aligned}$$

For sulfate anion, a similar computation can be performed and for the base case, this leads to:

$$\begin{aligned} \text{kg}(\text{SO}_4) &= \frac{237.76 \cdot (32.064 + 4 \cdot 15.9994)}{(6 \cdot 22.9898 + 2 \cdot (32.064 + 4 \cdot 15.9994) + 12.011 + 3 \cdot 15.9994)} & \text{(EQ 5)} \\ &= 160.8 \text{ kg}(\text{SO}_4) \end{aligned}$$

and when the sodium-sulfate-carbonate double salt is considered, to:

$$\begin{aligned} \text{kg}(\text{SO}_4) &= \frac{335.57 \cdot 2 \cdot (32.064 + 4 \cdot 15.9994)}{(6 \cdot 22.9898 + 2 \cdot (32.064 + 4 \cdot 15.9994) + 12.011 + 3 \cdot 15.9994)} & \text{(EQ 6)} \\ &= 165.3 \text{ kg}(\text{SO}_4) \end{aligned}$$

These results indicate that an experimental investigation of the kg sodium-sulfate-carbonate-hydroxide system is warranted to determine the impact of ionic strength on the solubility of the double salt as well as to determine the effect of ionic strength on the transition temperature for the double salt formation. The impact of ionic strength on the transition temperature in both the sodium carbonate system and the sodium sulfate system are well documented.

**TABLE 3. Comparison of solid phase speciation - inclusion of  $\text{Na}_6(\text{SO}_4)_2\text{CO}_3$  as potential solid.**

Species	Base Case Public + Trona + Na <sub>2</sub> SO <sub>4</sub>	Public + Trona + Na <sub>2</sub> SO <sub>4</sub> + Special Database
Total Solids (kg)	616.61	546.70
Al(OH) <sub>3</sub>	6.38	6.18
Ca <sub>3</sub> (PO <sub>4</sub> ) <sub>2</sub>	0.55	
CaCO <sub>3</sub>		0.53
Cr(OH) <sub>3</sub>	0.73	0.74
Fe(OH) <sub>3</sub>	0.54	0.54
Na <sub>2</sub> C <sub>2</sub> O <sub>4</sub>	0.43	0.44
Na <sub>2</sub> CO <sub>3</sub> ·1H <sub>2</sub> O	177.83	
Na <sub>2</sub> SO <sub>4</sub>	237.76	
Na <sub>6</sub> (SO <sub>4</sub> ) <sub>2</sub> CO <sub>3</sub>		335.57
Na <sub>3</sub> FSO <sub>4</sub>	24.05	19.50
Na <sub>7</sub> F(PO <sub>4</sub> ) <sub>2</sub> ·19H <sub>2</sub> O	130.46	142.45
NaNO <sub>3</sub>	37.89	40.75

Figure 19 provides a comparison of the sulfate predictions with the experimental data at 50°C. Again, from the experimental data, it is observed that a large fraction of the sulfate in the original saltcake is partitioned into the liquid phase at lower dilution levels. The ESP calculations indicate complete dissolution of the sulfate salts after approximately 250% dilution by weight, in contrast to the experimen-

tal data that indicate that the sulfate is found completely in solution after approximately 150% by weight diluent is added. While the sulfate is primarily found as anhydrous sodium sulfate in the model calculations performed for 25°C, at the higher temperature of 50°C, it is partitioned into the solid phase as the sodium-sulfate-carbonate double salt.

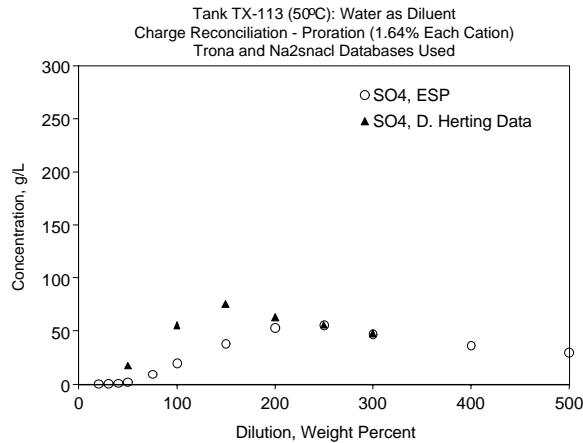


**FIGURE 19. ESP predictions and experimental sulfate concentrations for TX-113 saltcake at 50°C.**

**Comparison of model calculations with experimental results for phosphate and fluoride anions for TX-113 saltcake.** The TX-113 saltcake contains considerably more phosphate (3.75% by weight) compared to any of the saltcakes examined during previous years (.34 to .56% by weight). During sequential dissolution experiments performed by Herting, it was noted that the sodium- fluoride-phosphate double salt did not completely dissolve even after two sequential washes and thus, the amount of fluoride in this saltcake was estimated. Herting used the ICP results for phosphorus and for sulfur from the centrifuged solids remaining after the two sequential washes and estimated an upper bound for fluoride content of 0.60% by weight. Using only the IC data from the two sequential washes provides a lower bound of

0.28% by weight for the fluoride. This level of fluoride is in the mid-range for fluoride content of the saltcakes examined during FY 98 and FY 99 (0.07% to 1.17% by weight). Model results shown in Figure 20 were obtained using the upper bound as the fluoride input and although the fluoride concentrations are small, the general trend evident in the experimental data is mimicked by the ESP model calculations. The gradual rise in the experimental data is indicative of the presence of fluoride-containing species in the solid phase. ESP predictions indicate that these species,  $\text{Na}_3\text{FSO}_4$ , and  $\text{Na}_7\text{F}(\text{PO}_4)_2 \cdot 19\text{H}_2\text{O}$ , will persist in the solid phase until a 300% by weight dilution is achieved. Experimental dissolution results are limited to the range of 50 to 300% by weight, so experimental verification that complete dissolution of the fluoride containing species is achieved at higher levels of dilution (400%) is not available.

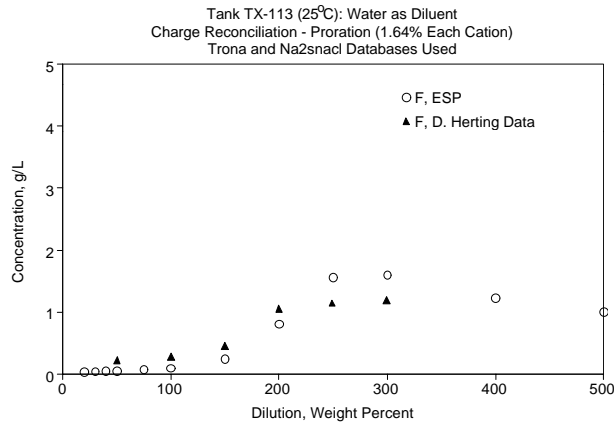


**FIGURE 20. ESP predictions and experimental fluoride concentrations for TX-113 saltcake at 25°C.**

In contrast to the fluoride-containing solids dissolution observed in the experimental data and predicted by the model at 25°C, the results at 50°C (Fig. 21) indicate that the model predicts solids dissolution at much lower diluent addition levels than found in the experi-

ments. In this case the model finds a maximum phosphate ion concentration at a dilution of 100% while the experimental maximum is observed at 250%. This behavior is under investigation; Further improvements to the ESP database for natrophosphate and for the  $\text{Na}_3\text{FSO}_4$  system are in progress.<sup>31</sup> Solid-liquid equilibria data for the Na-F-PO<sub>4</sub>-OH system has been sent to A. Hu at Hanford for fitting to the ESP employed Bromley formalism. Recent experimental results for the Na-F-SO<sub>4</sub>-OH system will be reported later.

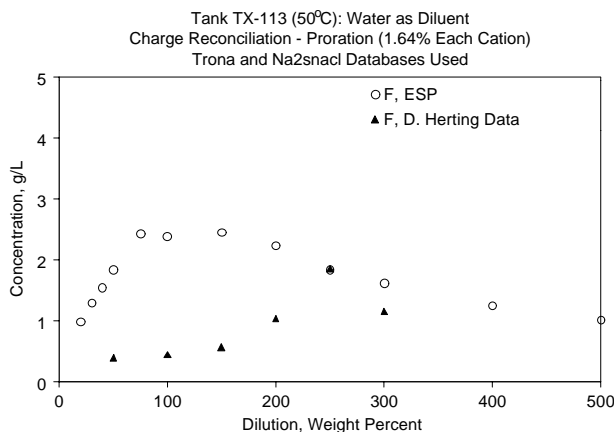


**FIGURE 21. ESP predictions and experimental fluoride concentrations for TX-113 saltcake at 50 °C.**

ESP predictions for phosphate concentrations at 25°C are shown in Figure 22. Again, the model calculations overestimate the phosphate concentration compared to the experimental measurements. The total phosphorus content in the liquid and solid phases predicted by ESP were calculated and compared with the phosphorus weight percent in the original TX-113 saltcake and found to be in agreement. For this saltcake, Herting<sup>29</sup> indicated that a considerable amount of the phosphorus present in the sample remained in the centrifuged solids phase after the two-step sequential dissolution. It is possible that the discrepancy between ESP predictions for phosphate concentra-

tions and the experimental measurements may be due to overestimation of the amount of phosphate in the original saltcake.

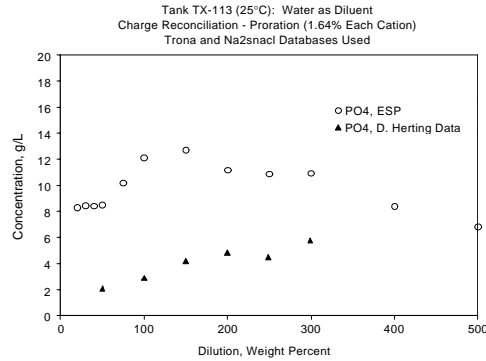


**FIGURE 22. ESP predictions and experimental phosphate concentrations for TX-113 saltcake at 25°C.**

As shown in Figure 23, the model predictions are seen to continue to underestimate the experimental phosphate ion solubility at the elevated temperature of 50°C. The questions raised in evaluating the 25°C data also apply at the higher temperature.

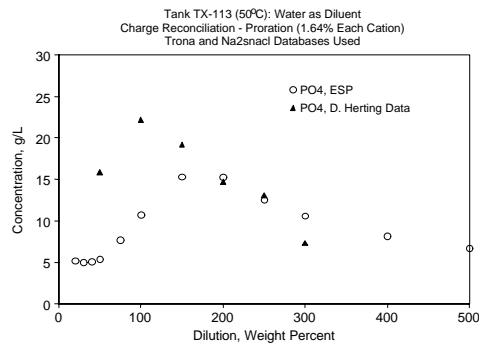


**FIGURE 23. ESP predictions and experimental phosphate concentrations for TX-113 saltcake at 50°C.**

**Comparison of model calculations with experimental results for nitrite, chloride and oxalate anions for TX-113 saltcake.** The amounts of nitrite, chloride and oxalate contained in the TX-113 saltcake are relatively low compared to the other anions present in this saltcake. In addition, compared to the four saltcakes examined in previous work, the weight percent for each of these anions is the lowest examined thus far. ESP predicts that both nitrite and chloride will be partitioned only into the liquid supernate and that no solid sodium nitrite or solid sodium chloride is present in the solid phase of the saltcake. Model predictions for nitrite concentration agree well with experimental data over the range of diluent addition examined and are shown in Figure 24. Similar agreement was observed in comparing the predicted and experimental nitrite concentrations at 50°C, Figure 25. For chloride, the low initial content (0.06% by weight in saltcake TX-113) compared to the range examined in earlier studies (0.11 to 0.41% by weight) may be responsible for the discrepancies observed in Figure 26 (at 25°C) and in Figure 27 (at 50°C) between model calculations and experimental dissolution data. The measured experimental concentrations do not exceed 1 g/L at any level of dilution.

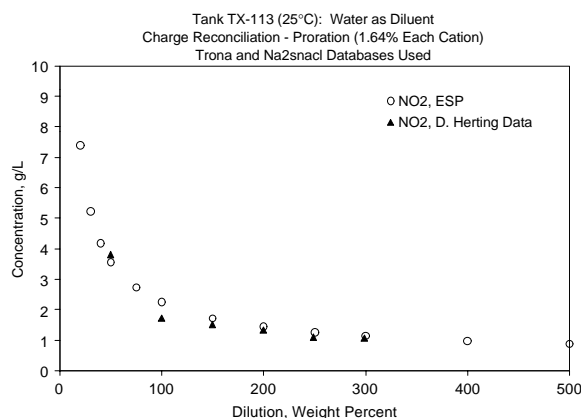


**FIGURE 24. ESP predictions and experimental nitrite concentrations for TX-113 saltcake at 25°C.**

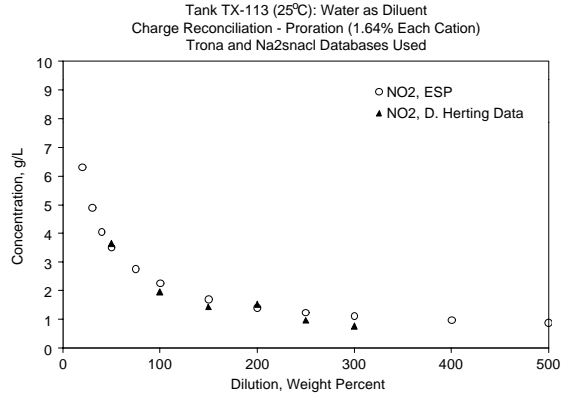


**FIGURE 25. ESP predictions and experimental nitrite concentrations for TX-113 saltcake at 50°C.**

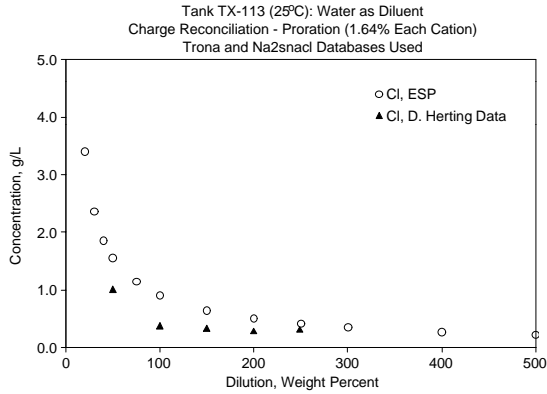


**FIGURE 26. ESP model predictions and experimental chloride concentrations for TX-113 saltcake at 25°C.**

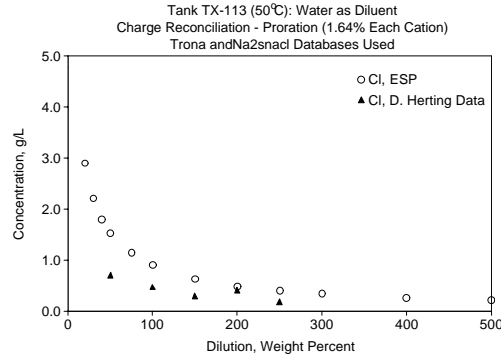


**FIGURE 27. ESP predictions and experimental chloride concentrations for TX-113 saltcake at 50°C.**

For oxalate, Figures 28 and 29, approximately one half of the analytical measurements resulted in reported concentration level below the detection limit of the instrument. Thus, any conclusion regarding reproducibility of experimental results by the model predictions is questionable. The predictive capabilities of ESP with regard to oxalate anion are better assessed through examination of experimental dissolution data from saltcakes with higher initial oxalate levels.<sup>26</sup>

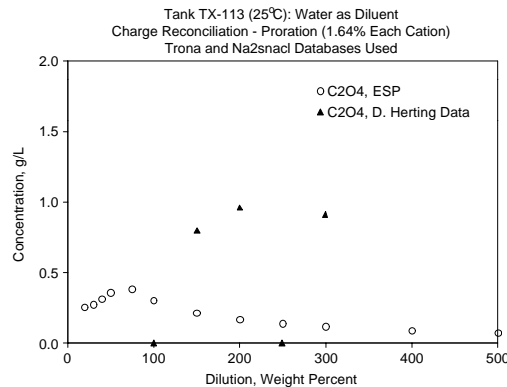


**FIGURE 28. ESP model predictions and experimental oxalate concentrations for TX-113 saltcake at 25°C.**

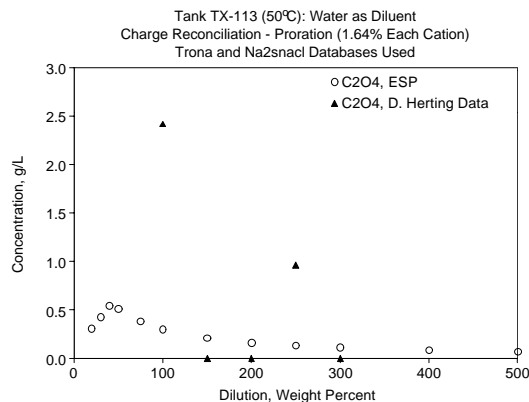


**FIGURE 29. ESP predictions and experimental oxalate concentrations for TX-113 saltcake at 50°C.**

## Conclusion

The choice of TX-113 saltcake for the FY00 dissolution studies was productive in terms of extending the knowledge base for ESP users at the Hanford Site. The high levels of sulfate in the saltcake led to the identification of inadequacies in the Public database for modeling the behavior of sodium sulfate salts in high ionic strength solutions. As a result, the OLI supplied database, Na2snacl, was incorporated along with the Trona database and used for all modeling reported herein. It is extremely important that these deficiencies be identified through comparison of model results to the experimental data, so that ESP can be used with confidence in staging retrieval operations at the Hanford site. The incorporation of the Na2snacl database significantly impacted the model results for the TX-113 saltcake. In addition, comparison to the experimental data and to the model predictions indicated that additional experimental data are needed for the sodium-sulfate-carbonate-hydroxide system. Using the Public database coupled with the two auxiliary databases for carbonate and sulfate does not significantly impact the solid phase predictions for saltcakes that are much lower in sulfate content.

## Project Status

Program execution guidelines have been developed for this program for work in fiscal year 2001 and 2002. Expansion of the work to include evaluation of the enhanced sludge washing process is included.

## Work Planned

Calculations for the feed stability experiments conducted at Hanford are currently in progress. Most of the experiments and thermodynamic simulations for the sodium-fluoride-sulfate-hydroxide system have been completed and will be documented. Work will be initiated on the sodium-sulfate-carbonate-hydroxide system. Experimental studies are also in progress on the solid-liquid equilibria behavior of sodium fluoride in the presence of nitrate and hydroxide.

## References

23. R.K. Toghiani, J.S. Lindner, C. Barfield and E.C. Beahm. 1998. Saltcake dissolution modeling, FY 1998 status report. DIAL-40395-TR98-1. Diagnostic Instrumentation and Analysis Laboratory, Mississippi State University, Mississippi State, MS.
24. R.K. Toghiani and J.S. Lindner. 1999. Saltcake Dissolution Modeling, FY 1999 status report. DIAL-40395-TR99-1, Diagnostic Instrumentation and Analysis Laboratory, Mississippi State University, Mississippi State MS (1999)
25. J.S. Lindner, R.K Toghiani and C Barfield. 1998. Thermodynamic simulation of Tank 241-SY-101 dissolution, part 1: in-situ crust dissolution. DIAL 40395-TR98-1. Diagnostic Instrumentation and Analysis Laboratory, Mississippi State University, Mississippi State, MS.
26. J.S. Lindner and R.K Toghiani. 1998. Thermodynamic simulation of Tank 241-SY-101 dissolution, part 2: supernate transfer followed by in-tank

- dilution. DIAL 40395-TR98-1.2. Diagnostic Instrumentation and Analysis Laboratory, Mississippi State University, Mississippi State, MS.
27. J.S. Lindner and R.K Toghiani. 1999. Thermodynamic simulation of Tank 241-SY-101 dissolution, part 3: crust solids dissolution modeling and associated gas release. DIAL 40395-TR98-1.3. Diagnostic Instrumentation and Analysis laboratory, Mississippi State University, Mississippi State, MS.
  28. D.L. Herting. October 1999. Personal communication.
  29. D.L. Herting. 2000. Saltcake dissolution FY 2000 status report. HNF-7031, Revision 0, Fluor Hanford, Richland, WA.
  30. R.K. Toghiani, J.S. Lindner, C.F. Weber, and R.D. Hunt. 2000. Modeling of sulfate double-salts in nuclear waste. ORNL/TM-2000, Oak Ridge National Laboratory, Oak Ridge, TN.
  31. J.S. Lindner, J. S. July 2000. Personal communication to A. Hu, CH2 Group Hanford.

---

## ***Solids Formation***

*J. S. Lindner, H. Al-Habbash and R. K. Toghiani*

### **Introduction**

Tank farm operations at Hanford include the interim stabilization program where the supernate and interstitial liquor in the single-shell tanks is reduced. Benefits from this process include the minimization of leakage from aging tanks, thereby limiting migration of waste into the soil, and the temporary reduction of waste within the tank. The process consists of jet-pumping the liquid in a given tank, obtained through a screen or salt well to a double-shell holding tank and then to an evaporator. Dilution water is added at the pump head. Recently, solids formation and plugging have been noted during transfers from

tanks 241-SX-104, 241-U-103, and 241-BY-102.<sup>32</sup> The primary solid responsible for the plugs from the first two tank wastes has been tentatively assigned, through experiments conducted on the waste liquid in the laboratory, as  $\text{Na}_3\text{PO}_4 \cdot 12\text{H}_2\text{O}$ . The plug formed during salt well pumping of BY-102 was believed to arise from sodium carbonate.

Other solids may participate in the plug formation process and this will largely depend on the solid-liquid equilibrium of the species contained in the waste stream. Little information, aside from the laboratory screening experiments is known regarding the mechanisms of plug formation and, more importantly, the required change in pressure that would indicate the beginning of plug formation. From operations measured records, the time needed for a plug can be determined and by knowing the pressures and flow rates the approximate location of the plug can be estimated; however, prevention of inadvertent plugs may be possible based on a suitable engineering tool that will allow operators to tailor waste transfers.

Development of an engineering tool that can describe slurry transfers and salt well pumping is also an objective of this program. In the case of slurry transport experimental data is being obtained at Florida International University and information on solids behavior, size, and growth rates is being measured at AEA Technologies. A test loop for obtaining data on supernate transfers does not currently exist. The lack of a test loop for salt well pumping, the need to understand the process in greater detail, and provide the fundamental data for development of the engineering tool provided the basis for the work described below.

## Work Accomplished

### *Results and Discussion*

Results are first described for the on-going experiments aimed at elucidating plug formation during Hanford salt well pumping operations. The second section of this section describes the development of the engineering tool needed by site personal to ensure safe waste transfers during retrieval operations.

#### *Salt well pumping flow loop experiments*

Details of the construction and testing of the laboratory-scale salt well pumping test loop and characterization of the 241-SX-104 surrogate stream were reported previously.<sup>33</sup> Additional characterization of the flow behavior of the surrogate and a number of experiments using the test loop are described.

#### *Viscosity of the sample 8 surrogate*

The viscosity is a critical parameter in the transfer of fluids. The formula for the surrogate sample was sent to ORNL for analysis using their Brookfield instrument. The viscosity is plotted against shear rate for measurements at different temperatures in Figure 30. Data points are shown for the measurement shear rate cycle. The data were initially obtained at low rates of shear and the speed of the rotor was increased to a maximum followed by decreasing the rate of shear to the original condition. Some hysteresis can be observed in the measurement cycles at the intermediate temperatures.

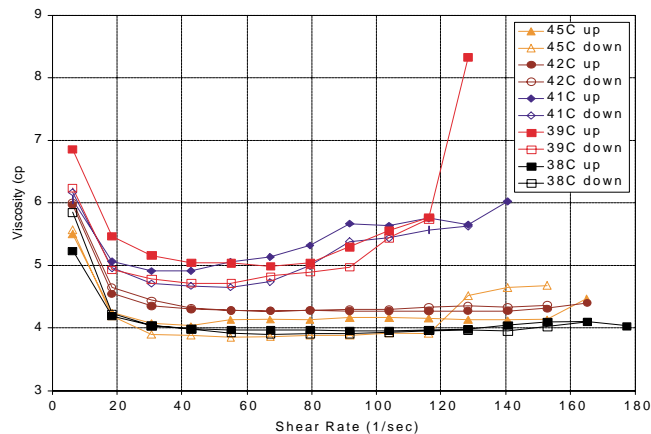


**FIGURE 30. Viscosity against shear rate traces for the sample 8 surrogate. The increase in viscosity at increasing shear rates is an example of shear thickening behavior.**

The curves all show an increase in viscosity at the lower shear rates indicative of non-Newtonian fluid flow. For the measurements at 45 and 42°C the viscosity does not significantly depend on shear at rates greater than about 30  $\text{sec}^{-1}$ . As the temperature is decreased to 41 and then 39°C the viscosity is seen to increase at shear rates above 50 - 70  $\text{sec}^{-1}$ . This behavior is consistent with shear thickening and probably represents ordering of the  $\text{Na}_3\text{PO}_4 \cdot 12\text{H}_2\text{O}$  rods. On decreasing the temperature further to 38 and then 36°C (latter not shown) the viscosity again becomes independent of shear at rates greater than 30  $\text{sec}^{-1}$ . It is believed that the decrease arises from solids or gel formation below the rotor of the viscometer or on the walls of the sample holder. Partitioning of the fluid in this manner would lead to a decrease in the overall solution viscosity. Similar results were observed previously in the ORNL parametric viscosity study.<sup>34</sup>

The shear thickening behavior observed for the sample 8 surrogate implies that specific flow rates or Reynolds numbers may need to be avoided at certain waste stream temperatures.

*Experiments on plug formation*

Upgrades to the salt well pumping flow loop have been made during the course of this work. The configuration of the loop has been described previously and will not be repeated here. In brief, the system was designed to effect the same Reynolds numbers, ( $ReD = DV\rho/\mu$ , where  $D$  is the channel diameter,  $V$  is the linear fluid velocity,  $\rho$  is the surrogate density, and  $\mu$  is the viscosity) observed during operations at Hanford. The system consists of an input surrogate tank and pump and a flow meter controls the rate of surrogate to the channel. Four tube-in-shell heat exchangers are located along the channel. Pressure transducers and thermocouples are located along the flow train and for monitoring the inlet and receiving tanks. Positions of the sensors along the flow train are given in Table 4.

**TABLE 4. Locations of thermocouples (T) and pressure transducers (P) along the channel.**

Sensor Meter (cm)	Distance from Inlet Flow
T1	10
T2	90
T3	177
T4	264
T5	351
P0	84
P1	170
P2	258
P3	344

Following the initial experiments it was noted that the optimal facility location where the plug should be generated was between heat exchanger 3 and heat exchanger 4. Upon plug formation the pressures upstream of the blockage would be at maximum values and downstream of this location the pressures would tend to lower values.

In a typical experiment, 18L of the Sample 8 surrogate was prepared and held at 70°C until all of the solids had dissolved. The contents of the tank were then cooled to 50°C. The surrogate recipe contains aluminum and by lowering the temperature of the supernate to 50°C the formation of gibbsite ( $\text{Al}(\text{OH})_3$ ) was minimized. Multiple experimental runs were performed with the initial composition. The sample channel was pre-heated with hot water from a water dilution tank to a temperature of about 60°C. Increasing the channel temperature in this way reduced the formation of gel particles on the inner wall of the channel. The loop was then drained and the surrogate flow started at a desired rate. The liquid was allowed to flow in the channel and then to the receiving tank where it was collected prior to transfer back to the holding tank. Temperatures were allowed to stabilize with no forced cooling. When the temperature at T4 reached 46°C the water to the third heat exchanger was started. Experiments were performed at a constant Reynolds number for different cooling rates. Additionally plug formation tests were carried out at different Reynolds numbers with a constant flow to heat exchanger 3 of 1.2 gal/hr. Additional experiments where the starting temperature is different from 46°C are planned.

#### *General data observations*

Pressure and temperature traces for an experiment with a surrogate flow rate of 4.8 gph and an exchanger 3 cooling water flow of 0.1 gpm are given in Figure 31. The data shown are for the period after heat exchanger 3 was activated. Temperatures for all locations on the channel and for the holding tank are shown along with the inlet cooling water temperature (TCW) and the exit temperature of the water from heat exchanger 3. Small variations in the tank temperature and for thermocouples 1 - 4 arise from the cycling of the immersion heater in tank 1. Thermocouple 4 is located between heat exchanger 3 and heat exchanger 4 and this position illustrates the change in temperature that is associated with plugging.

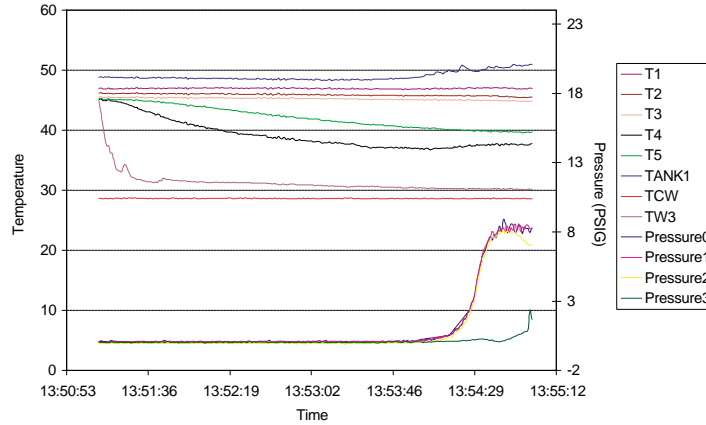


**FIGURE 31. Pressures and temperatures recorded for the experiment on 8/22/00. The surrogate flow rate was 3.5 gal/hr and the water to heat exchanger 3 was metered at 0.1 gal/min**

Of interest are the pressure increases that start around 13:54 and continue until reaching a maximum value indicative of complete line blockage. The location of the pressure transducers, Table 4, confirms that the plug was established between heat exchanger 3 and heat exchanger 4. A reading was not observed on the flow meter following formation of the plug. The maximum pressure that was observed depends on the pump. The downstream pressure transducer shows a delayed increase and this is due to the higher downstream temperature that reduced the rate of formation of the phosphate rods.

From the data in Figure 31 the general properties of plug formation, such as time to plug, the fluid temperatures after plug formation, temperature drops, and overall pressure increases can be obtained. A list of the experiments and the data and the averaged parameters are collected in Tables 5 and 6. Heat exchanger thermocouples were only

installed for the last two experiments. In this case more information regarding the heat transfer properties of the flow can be obtained.

**TABLE 5. Characteristics of the initial experiments.**

Date	Surrogate Flow (gal/hr)	HEX 3 Cooling Water (gal/min)	Re	T4 Rate of Temp Change (C/sec)	Time to Plug (sec)	Pressure at Plug (psig)	T4 at Plug (C)	T5 at Plug (C)
8/11/00	3.5	0.10	223	0.044	294	9.0	38.3	38.4
8/18/00	3.5	0.10	223	0.051	222	8.3	37.6	39.7
8/23/00	3.5	0.10	223	0.063	288	8.5	43.1	41.0
8/10/00	3.5	0.66	223	0.073	268	8.9	38.8	39.7
7/21/00	3.5	1.20	223	0.153	264	8.0	38.8	39.4
8/14/00	3.5	1.20	223	0.055	248	8.6	40.6	40.1
8/17/00	3.5	1.20	223	0.048	250	8.6	39.4	39.8
7/21/00	5	1.20	319	0.087	692	7.7	43.5	42.5
7/24/00	6.8	1.20	436	0.073	2656	7.7	46.0	45.2

**TABLE 6. Average values for the experimental conditions.<sup>1</sup>**

	Time to Plug (sec)	T4 at Plug (C)	T5 at Plug (C)	Pressure at Plug (psig)	Change in T4 (C)	Change in T5 (C)
<b>Data for All Runs</b>						
Average	NA	40.7	40.6	8.4	5.4	5.1
STD	NA	2.9	2.1	0.5	2.5	1.9
STD Error (%)	NA	7.0	5.0	5.5	47.0	37.2
<b>Data for Re = 223</b>						
Average	262.0	39.5	39.7	8.6	6.2	5.9
STD	24.8	1.8	0.8	0.3	2.1	0.9
STD Error (%)	9.5	4.7	2.0	3.8	33.5	15.3
<sup>1</sup> Data on pressure and temperatures is at complete plug formation.						

From Table 4 it appears that only minor variations in the measured experimental parameters were observed for the lowest Rey-

nolds number experiments. At the lowest Reynolds number, the time needed to form a plug did not depend on the rate of temperature decrease for the range of decreases tested. Averages shown in Table 6 for many of the parameters indicate small variations for all of the experiments irrespective of cooling water rate. Results for the time to plug at  $Re = 223$  indicate that the plug was formed at a similar channel location based on the constant inlet stream velocity and the pressure profiles. A main observation from the data is the increase in the time needed to form the plug at the higher surrogate flow rates.

Although the pressures at  $Re_D = 319$  and  $423$  are somewhat reduced as compared to the average values when all of the data is considered (compare Tables 5 and 6), the results are within  $\pm 2$  standard deviations of the overall average. Similar comments apply to the temperatures recorded by the thermocouple close to the plug formation location (T4) and that temperature located downstream of the plug at T5. Here (Table 5) the final temperatures increased over those observed during the low flow rate experiments; however, the data are still within the statistical criteria.

The lack of a statistically significant trend on the cooling water flow can be traced to the size of the heat exchanger with respect to the channel diameter. It is believed that lower cooling water flow rates will be necessary to observe the effect. Provisions have been made to install smaller flow meters on the heat exchanger and these will compensate for the large size (with respect to the channel diameter) of the module. Alternately, the thermal characteristics of the surrogate are expected to change as the baseline composition is diluted. This, along with increasing the Reynolds number of the experiments, provides an additional way to evaluate cooling rate effects. Changes in the stream temperature from the starting values until plug formation, Table 6, do not seem to exhibit a significant effect over the formation process. Here, however, it should be remarked that the heat exchanger was activated for all of the experimental runs when the surrogate temperature reached  $46^\circ\text{C}$  at T4. Starting the heat exchanger at a different

stream temperature may or may not have a significant effect depending on the heat exchanger flow and the surrogate dilution level and composition.

*Comparison of experimental results for different Reynolds numbers*

Pressures and temperatures for the runs at different Reynolds numbers with a constant cooling water rate to heat exchanger 3 of 1.2 gal/min, are plotted in Figures 32 and 33. The results were taken from the experiments conducted on 7/21/00 (Run 9 and Run 12,  $R_{eD} = 223$  and 319) and the experiment on 7/24/00 (Run 13,  $R_{eD} = 436$ ). The data for Run 13 has been shifted for presentation by the addition of a constant factor. The temperature traces observed for the lowest surrogate flow rate show a rapid decrease as compared to the intermediate and higher flow rates where a constant temperature is observed prior to plug formation. Once the plug forms the temperature decreased.

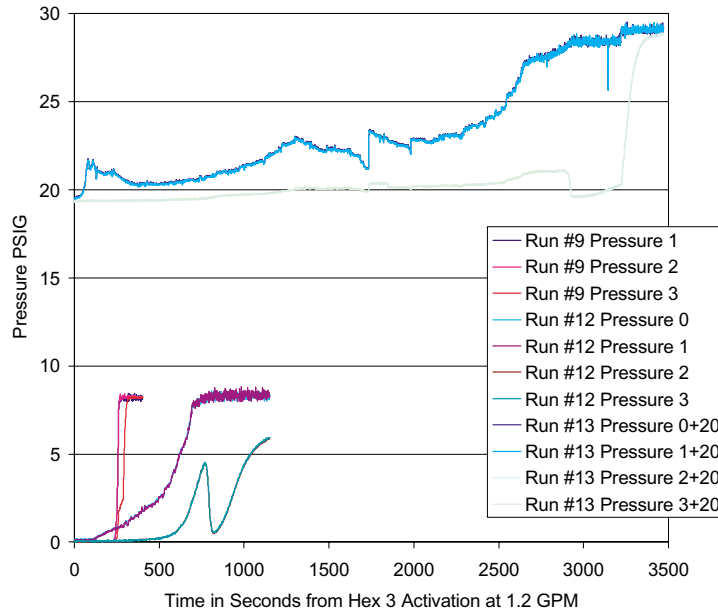


**FIGURE 32. Pressures for the experiments at different flow rates.**

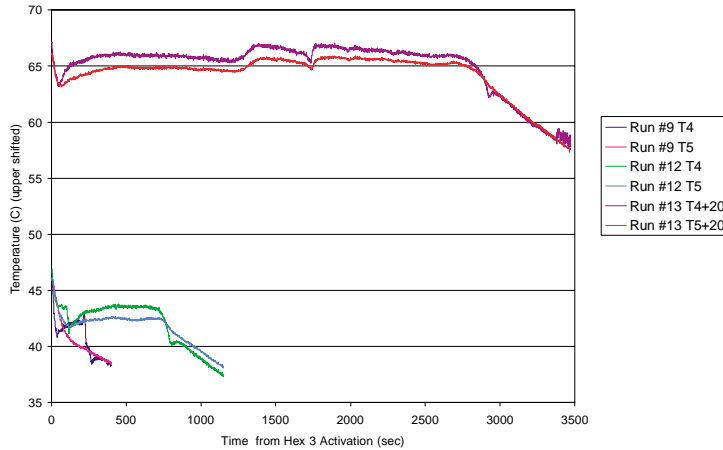


**FIGURE 33. Temperatures for the experiments at different Reynolds numbers**

The pressure traces indicate that plug formation was more gradual at the higher Reynolds numbers. A delayed increase in pressure was observed at  $R_{eD} = 319$ , as compared to the  $R_{eD} = 223$  run, and an even more gradual pressure rise was found at the highest surrogate flow rate investigated. The data for run 13 (7/24/00) show an initial increase in pressure followed by a decrease and then a small increase eventually resulting in plug formation. The trace is believed to represent fouling of the channel over time. The pressure data also indicate different plug locations. For the lowest and highest surrogate flows a plug was formed shortly after heat exchanger 3 and eventually extended downstream. The plug for  $R_{eD} = 319$ , Run 12, also formed following heat exchanger 3 but development of a downstream plug was delayed. The thermocouple temperatures at T4 and T5 signify the difference in the location of the plugs. These values are the same for Runs 9 and 13 but for Run 12, T4 never equals T5. In most cases the average values of T4 and T5 were the same (Table 5). The reason for the difference in the temperatures observed during Run 12 are not known but may relate to the length of the plug formed and the associated mass balance between the initial plug formation location and the material available to form the plug at the downstream location. In

addition, cycling of the immersion heater in the feed tank will alter the downstream channel fluid temperatures.

*General flow characteristics, heat capacity and dimensionless numbers*

Analysis of the data indicates that the primary variable responsible for the time to plug is contained in the definition of the Reynolds number,  $R_{eD} = DV\rho/\mu$ .  $R_{eD}$  will begin at a known value and eventually become zero upon completion of the plug. The path for the change in the Reynolds number will not necessarily be linear since changes in the density, velocity, and viscosity can take place as the plug is forming. The density of the surrogate waste was calculated from ESP as 1.39 Kg/L at 40°C. The density of solid trisodium phosphate is 1.62 Kg/L. Assuming that the plug is solid TSP, the stream density would only increase by ca. 17%. The total solid loading upon gel formation is only 0.68% by weight so the change in the density is not significant.

It is somewhat more difficult to assess the effects of the velocity and the viscosity. If the flow remains laminar and constant, the change in pressure can be expressed as

$$\Delta P = \frac{(32\mu V)}{d^2} \quad (\text{EQ 7})$$

where  $d$  is the inner diameter of the channel. Examination of the experimental data (Figs. 32 and 33) indicate that for some period of time the pressure remains at a reduced value compared to that observed after complete channel blockage. This time may be related to an induction period where the rods are starting to form but are not of sufficient size or number to form the gel. During this time the changes in  $V$ ,  $\mu$  and  $d$  are not sufficient to increase the pressure above the baseline value.

At plug formation, the pressure is at a maximum and the channel diameter available for transport of the surrogate stream becomes 0. During plug formation the pressure increases. Surrogate metered into the channel remained at a constant flow rate until just before reaching the limiting pressure. The local viscosity is considered to be the same as that measured at the plug temperature, thus  $\Delta P \propto K/d^2$ , where K is a constant.

The time needed to form the plug depends on the Reynolds number and from the above expression the governing parameter is the linear fluid velocity. Although additional data is needed, it appears that increasing the velocity will reduce the time available for interaction of the rods with one another. Intramolecular interactions are necessary to assemble the three-dimensional gel structure; the gel is not formed from covalent bonds and as the stream velocity increases, the contact time between the rods may decrease owing to additional transport forces on the rods. In essence, the additional molecular velocity at the higher flow rates reduces the number of “sticky collisions”. This explanation would amount to a preferential orientation of the rods at higher velocities.

The results obtained thus far imply that from a practical standpoint the transport of salt well liquor under constant cooling conditions will be more successful at higher flow rates. Little discussion has been placed on the thermal effect associated with the experiments. It is quite clear that the extent of cooling of the fluid will determine the number of TSP rods formed and this, in turn, will set the gel formation point. The heat capacity of the sample 8 surrogate was determined using the flow loop. The specific heat was determined based on heat balance as  $\sim 3400$  J/gK. This result is within 9% of that value (3100 J/Kg.K) obtained from the enthalpies calculated using ESP

Dimensionless quantities are currently being evaluated with regard to the experimental results. The search for a suitable dimen-

sionless number was initiated in an attempt to find terms that could be directly employed by engineers at Hanford. A number of observations make this analysis involved. First, at low Reynolds numbers the plugging process is extremely rapid. Formation of the plug does not following a traditional sedimentation pattern. Rapid growth of the TSP crystals has been observed.<sup>34</sup> Laser diffraction experiments, conducted at AEA, were unable to follow the kinetics of the process.<sup>34</sup> Additional experiments are needed to further understand the plug formation process and translate the pertinent variables into working expressions.

Even calculation of the Prandtl number,  $(C_p\mu/k)$  where  $k$  is the thermal conductivity, is hindered by the behavior of the viscosity. For the experiments plotted in Figures 32 and 33 the associated shear rates vary from 130 to 253  $\text{sec}^{-1}$ . Viscosity data is available ca. 130  $\text{sec}^{-1}$  at 41 °C and appears to be increasing (Fig. 30). Other dimensionless parameters such as the Brinkman and Ellis numbers are under evaluation, but here as well, additional viscosity data is needed. A sample has been prepared and submitted for analysis.

#### *Feed stability and prevention of solids formation model(s)*

Department of Energy (DOE) waste pretreatment and retrieval activities at Hanford have suffered from several delays in their transport operations due to plugging in transfer lines.<sup>32</sup> These activities include two distinct types (from a fluid mechanics point of view) of transport processes. The first involves the movement of supernates (salt well, SW, pumping and concentrated evaporator brines) and this type of flow is initially characterized by negligible or low solids concentrations. The second process involves the transfer of waste slurries (ST) where solids are present at moderate to high concentrations mostly at less than 20% by volume. Pipeline plugging in both operations results from the unintentional formation or deposition of solids during transport.

The main aim in this work is the development of an engineering tool that will accurately and efficiently predict particle deposition and plug formation while taking into account the dynamic behavior of the waste transport processes and, in so doing, reflect the impact of the waste chemistry. Once validated using data from companion work on laboratory and pilot-scale flow loops, the package will be tested at Hanford, upgraded if needed, and eventually transferred to site operations to help the operators minimize possible delays due to plug formation in transfer lines.

The physical processes that have to be taken into account to model particle deposition and plug formation in both the salt well pumping and pipeline transfer processes are similar and include fluid transport properties, heat transfer, chemical reactions, phase change, particle growth, agglomeration and particle settling and adherence dynamics. Despite these general similarities, the mathematical formulations needed to accurately represent the transport of multi-phase fluid flow differ.<sup>36</sup> At low solids concentrations, the usual practice is to use an Eulerian/Lagrangian formulation.<sup>36</sup> In this case the Eulerian framework is used to account for the continuous (carrier) phase, and the Lagrangian formalism is used to represent the dispersed/dilute phase as particles start forming in the flow. On the other hand, for simulations involving solids present at high volume fractions, usually more than 5% by volume, an Eulerian/Eulerian formulation is considered for both phases. This is due to the presence of high concentration of solids in the flow and the inefficiency of the Lagrangian formulation in accounting for particle/particle interactions and the two-way transfer of mass, momentum and energy between phases. In particular, how the dynamics of the dispersed phase influences the dynamics of the carrier phase.

In what follows the specific desired characteristics for the engineering tool, the modeling approach based on these requirements, and a description of the overall model are given. Results are then presented describing the initial efforts in assembling the model and in

evaluating the performance of the main transport module. Here simulations were conducted based on a WSRC surrogate composition previously evaluated in the slurry flow test loop at Florida International University (FIU).<sup>37</sup> Details of the calculations and a comparison with the experimental results are given. On-going model development activities are then described.

*Engineering tool objectives, requirements and approach*

Prior to and shortly after this work was begun, a number of objectives for the engineering tool were identified. These stem largely from the need at the site for the safe and efficient transfer of wastes. Delays in meeting scheduled deliveries can, depending on contractor requirements and inter-agency agreements, result in fines or action to DOE.<sup>32</sup> Currently only one cross-site transfer line is available to move waste from the 200 West to 200 East areas.<sup>32</sup> Plugging the transfer line would severely impact vitrification operations and delay, further, the remediation of the waste.

*Model objectives*

The requirements for the engineering tool were derived directly from the objectives, and from these it became possible to develop the modeling approach. The section below describes these analyses, the model configuration, and the data requirements. Goals for the engineering tool are listed below. The model must:

- be capable of predicting the formation of a plug in a transfer line for both ST and SW operations;
- allow the determination of the location of a plug and the approximate time needed to form the plug;
- predict the values of variables that are measurable by the Tank Farm Operators such as flow rates, pressures, temperatures and species concentrations etc.;

- be practical in terms of operator expertise to setup and run the model for a specific site transfer;
- be modular to optimize and minimize computational times.

*Model requirements*

As a starting point and without taking into account possible simplifications and/or the use of experimental data and correlations, the physical processes and properties that may have to be accounted for to accurately predict the fluid transport process, sedimentation, and plug formation are as follows:

- Number of species present in the flow field;
- Concentration of each species;
- Fluid properties, (flow rate, pressure, density, viscosity etc.);
- Conservation of mass of all species;
- Conservation of momentum for all phases, between phases and of all species;
- Conservation of energy and heat transfer in the flow field and between species;
- Chemical reactions between species and the formation of solids (all types of reactions should be accounted for until more simplifications are possible);
- Solid particle size, shape and density;
- Solid particle population balance and growth kinetics;
- Phase equilibria;
- Effects of chemical reactions and phase changes on the flow properties;
- Particle sedimentation, agglomeration and adherence behavior.

The above elements are to be incorporated and assembled in the overall model(s) by means of separate (in terms of the set of mathematical equations solved) modules. Each module will be responsible for calculating and/or correlating a specific process in the flow field. All of the modules will be assembled in an integrated package.

#### *Modeling approach*

The process by which the model is going to predict plug formation in a transfer pipe will require the solution of several highly complicated partial differential equations that describe the physical processes occurring during the transport.<sup>38</sup> This solution is carried over the entire flow field as a function of position or space (x,y,z) and time. The solution process starts by discretizing the governing partial differential equations of mass, momentum and energy for one or multiple phases (Eulerian or Lagrangian) over a finely spaced grid that spans the entire flow field. This grid is necessary to accurately define (in a discrete form) the geometry of the flow field and to apply the physical boundary and initial conditions. As the solution proceeds over the flow field (in space and time) the model will also require a means by which the results from the solution are accurately interpreted and understood.

The subjects of grid generation (preprocessing) and results interpretation (postprocessing) require a great deal of special expertise and time consuming development which adds considerably to the model complexity. In addition, the development of a thoroughly tested and verified computational fluid dynamics code is known to consume long periods of time and requires highly specialized expertise. Due to those reasons the modeling approach in this work is based on using a simple but yet general purpose CFD system; thereby, taking advantage of established capabilities. The work will then proceed with the addition of the required modules and assessing parameter significance. This approach is believed to allow for a reduction in development time.

A flowchart for the proposed model is given in Figure 34. The equations that are pertinent to the function of some of the modules (described below) have not been formalized yet owing to possible modifications.



FIGURE 34. Model flow chart.

**Input module.** The main role of this module is to provide a means by which the flow field geometry (pumping distance, junctions, valves etc.) is defined, the necessary grid for the solution is generated and the physical boundary and initial conditions are applied. The initial and boundary conditions consist of the already known properties regarding the waste composition and the waste transfer process. The former data may consist of a subset of the chemistry of the waste or a more detailed description. The later data

comprises temperatures, pump pressures, flow rates and geometrical data.

**Chemistry module.** The accurate prediction of the types and amounts of solids that could form in the (SW) and the total solids concentration in the (ST) for the given pumping process is essential for determining if a plug could form. Determination of the solids partitioning requires accurate calculations and well-tested/verified data. This is especially important for the waste streams under consideration here. The solids prediction module can be bypassed or substituted by available correlations/curve fits of experimental data or calculated, by, for example, the ESP program. Output from this module consists of the densities of the solids, the viscosity of the supernate, heat capacity, thermal conductivity, solids speciation and loading, and other critical supernate species that may participate in future particle formation.

**Particle growth/nucleation module.** The shape of the particles and the associated size will have a direct effect on plug formation. The particle shape, size and mass impact the transport dynamics, which has a direct connection to the critical particle velocity and deposition behavior. Additionally, under certain conditions the particle loading may increase or decrease depending on the temperature, solid-liquid equilibria, and kinetics. This will also have a direct impact on the fluids bulk viscosity.

**Bulk viscosity.** two distinct coefficients of viscosity are needed to describe the laminar flow of a two/multi-phase fluid. Of these coefficients the shear viscosity  $\mu$  is the more familiar. It describes the resistance of the fluid to changes of shape. The bulk viscosity describes the irreversible resistance over and above the reversible resistance given by the isotropic bulk modulus, to changes of volume. The effects of bulk viscosity can be ignored for dilute monatomic gases and for simple incompressible fluids. As the solids concentration in the fluid increases, the bulk viscosity starts to have a direct effect on particle transport and must be calculated as a function of flow proper-

ties and particle formation. This module could be substituted by experimental correlations (as they become available) which can be used as an input to the module containing the equations that govern the fluid flow.

**Transport module.** provides calculation of the pertinent quantities relating to plug formation and process operation. This module can be divided into two sub-modules as shown in the figure.

- The first sub-module to the left, indicated as Transport module, the continuum/Eulerian partial differential equations governing the fluid transport process are solved. These equations consist of a set of mass, momentum, energy and (when needed) turbulence conservation equations for each phase available in the case of flows with high solid content. Or only one set of mass, momentum and energy equations for the continuous phase in the case of flows with zero or low solids content. It will also calculate particle population balance, deposition velocity and settling or adherence position (if any) in the flow field as the simulation develops. This module is the largest and most involved and consists of many subprograms that perform specific functions.
- The second sub-module to the right indicated as, Particle Dynamics and Tracing, can be used for two different roles. It provides for the description of particle dynamics and their interaction and the resulting effects on the continuous phase for those situations where particle loadings are low. The second role it plays for both the (ST) and (SW) by providing a mechanism to dynamically tracking the solid particles in the flow field as they grow and/or agglomerate and ultimately under adverse conditions form a plug. The particle growth kinetics and tracking modules are essential for modeling the low solids supernate pumping operations and believed to be computationally very intensive even for a two-dimensional simulation.

The modules are executed in the sequence presented in the figure. Calculations are performed iteratively over the whole flow field as a function of time with recourse to the fundamental SLE of the system. The results from the Transport Model are evaluated after each time step to determine if, where, and when a plug will form along the transfer line. If a plug has not been formed but yet suspected the program proceeds to the next time step until additional development is observed. The user can then change (if necessary) the initial pumping parameters (add water or increase the flow rate etc.) and restart the simulation once again. If the flow field has been completely evaluated and a plug has still not been observed then the composition of the waste and the engineering parameters are consistent with safe transfer.

Advantages of the proposed approach are the modularity (some calculations can be bypassed if not needed) and the ability to initially develop correlations from laboratory experiments that can transfer results directly to the Main Transport Module.

Efforts will be devoted to the simplification and/or elimination, when possible, of some of the modeling parameters (dimensions, chemical processes, kinetics, etc.) based on the results gained from the accompanying experimental effort(s) and experience, as they become available. Those findings should give a clearer view and greater insight to which of the modeling parameters play a major role and have to be completely accounted for and to which that can be simplified, correlated or even ignored.

Description of the physical processes inherent to particle deposition and eventual plug formation are thought to require a considerable amount of information. As noted in the flowchart and the previous discussion, a large portion of this data will be specific to the experiments scheduled as part of the overall Prevention of Solids Formation Program. These parallel efforts are being performed at ORNL, AEA Technologies, Florida International University, and DIAL/Mississippi

State University. The model development philosophy is based on a multi-phase approach and will initially focus on surrogates from Hanford tanks 241-AN-103 for slurry transfer and 241-SX-104 for salt well pumping.

Workers at FIU are performing slurry transfer and plug formation experiments in a pilot-scale closed loop system. The FIU studies can provide data needed to develop and validate the model especially the Main Transport Module for the ST process. This information will include:

*Module/model inputs*

- Slurry composition data, solids loading, slurry density, supernate viscosity.
- Particle Size/shape/growth characteristics.
- Bulk viscosity of the slurry.
- Geometry information on pipe diameter, length, temperature and heat tracing characteristics.
- Pressures, pressure drops and flow rates a function of time.
- Thermal characteristics of the process (temperatures, thermal conductivities, heat capacities).
- Fluid/particle velocities.

*Module/model comparisons*

- Time needed to form a plug under specific operating conditions.
- Characteristics of the plug, i.e., location, solids composition, etc.

Additional information will be available from AEA Technologies on particle size, growth, agglomeration and disruption studies for the AN-103 surrogate. These results could be used to replace the particle

growth module. As part of this work MSU/DIAL will perform solid-liquid equilibrium calculations on the surrogate. This will provide the data necessary to initiate model development activities for the Main Transport Module. The data can then be compared to the AEA and FIU results on the solids formed and the pertinent volume fractions.

Workers at ORNL are performing viscosity experiments for the (SW) process and developing viscosity correlations using a neural-network model for the prediction of bulk viscosity and rheology. The neural network results will not be available for incorporation into the viscosity module during FY 2000. The waste feed stability subtask at ORNL is also developing sub-models that can be used in our rigorous simulations, and is developing simplified macroscopic balance models of waste transport.

As another part of the overall Prevention of Solids Formation Task work was initiated on the development of a laboratory-scale test loop for saltwell pumping. The validation data for the development of a SW model will largely come from this system. Data requirements are the same as those for the ST model with the exception that solids will not initially be present in the SW liquor. Runs have been conducted with SX-104 simulant and are planned for U-103. Parallel activities at ORNL and AEA will focus on the SX-104 surrogate.

The viscosity studies on the SX-104 surrogate from ORNL and the particle size/nucleation experiments from AEA will be employed. MSU/DIAL will perform SLE calculations for both the model and test loop development. The data will be transformed into correlations to streamline and allow concentration on the main transport module.

#### *Evaluation of commercially available codes*

Prior to the development of the current modeling approach a preliminary study was developed to determine what other multiphase slurry transport models were available. Helix technologies offers the

Delta Q program that allows the calculation of the critical settling velocity for slurries with various particle size distributions.<sup>39</sup> Initial calculations based on particle information indirectly obtained from ESP and studies conducted previously at FIU indicated that the critical settling velocity could be calculated to within 5%. This code, however, falls short in addressing all of the current model requirements in that the formation of a plug does not consider the potential reacting nature of the flow, heat transfer is not formally considered, and the model is only one-dimensional.

Other software has been noted, specifically the work of PNL with the TEMPEST code.<sup>40-42</sup> TEMPEST is a powerful analysis tool and is capable of performing simulations in two and three coordinate dimensions with account for mass, momentum and heat transfer for incompressible flow. It is available in N and T-versions. The T-version has more capabilities and is not available to the public. The main drawback related to the current work is that the TEMPEST lacks built in (to our knowledge) capabilities for particle tracing, particle growth kinetics, particle/particle interaction and changes in bulk viscosity due to solids formation that are necessary for the SW model. Additionally, the available N version of the code is restricted to cartesian or cylindrical coordinates and lacks pre/post-processing capabilities.

These studies when compared to the modeling requirements resulted in the proposed model as depicted in the flow chart of Figure 34.

A number of commercial computational fluid dynamics packages that are capable of simulating complex transport processes are available; i.e., FLUENT 4.5 and 5.0 from FLUENT Inc., CFD2000 from SIMUNET Corp., PHOENICS 3.3 from CHAM Ltd., CFX 4 and 5 from AEA Technology, FLOW 3-D from Flow Science Inc., and STAR-CD from Computational Dynamics Ltd. (among others). These codes are well tested, validated and documented. Most of these companies integrate preprocessing and postprocessing programs into

their packages without the need for other programs to produce complete simulation and prediction results. None of these codes, however, contains all of the physics for the proposed model.

After careful and thorough search and comparison of the available CFD software with our requirements a decision was made to obtain the PHOENICS 3.3 package from CHAM Limited. The codes strongest attraction for the current modeling effort is the fact that most of the flow solver part of the program is available in an open source code format where it can be modified, optimized and tailored or completely changed. The code has been used to study single, two and multiphase flows with Eulerian/Eulerian and Eulerian/Lagrangian descriptions for the two and multiphase materials and several different turbulence models are available. Simulations are obtainable for most types of flows on simple and complex geometries in cartesian, cylindrical and curvilinear body fitted coordinates. From an end-user perspective the code can be run using a graphical user interface (Virtual Reality Editor) by choosing from a preprogrammed collection of simulation cases tailored to the specific tank farm operations needs. This will not require more than being familiar with inputting some numbers concerning the pumping operation in progress like dimensions, compositions, concentrations, flow rates, etc.

#### *Preliminary code testing*

The PHOENICS code version 3.3.0 arrived at DIAL/MSU around the end of April 2000. It was immediately installed on the available PC system which had a Pentium II class microprocessor. Standard tests were then performed involving: (1) geometry definition, coordinate system and grid generation for simple shapes; (2) solver setup; flow model, associated physics, initial and boundary conditions definition and solution execution; and (3) results manipulation, visualization, analysis and verification

The software simulation setup process (for simple flow with simple physics) was systematic with easy to follow steps and with a limited guidance from the software. Due to time and effort constraints only a few of the relevant code capabilities have been examined so far.

*Early model development, simulations and results*

The proposed model as shown in Figure 34 above contains several modules. The best approach to insure its proper function and validity is to build and test each module separately, if possible, as it evolves. PHOENICS will mainly represent the transport and probably the particle dynamics modules. As customary with any new predictive software tool it was deemed necessary to perform a series of simulations on two/multi-phase flows that start with simple but relevant physics and gradually increase in complexity. The results are then compared with available data.

In a related work, researchers at FIU experimented with SRS slurry C simulant that consisted of a carrier fluid with solid particles of two sizes, Table 7.<sup>37</sup>

**TABLE 7. Characteristics of FIU slurry C.**

	Density (Kg/m <sup>3</sup> )	Viscosity (cp)	Diameter (μ)	Concentration by (% volume)
Carrier Fluid	1005	0.913		92.4
Particle 1	3147		45	2.9
Particle 2	3147		220	4.7

The FIU experiments were related to Slurry transfer and particle settling velocity. The settling of particles is believed to play a major part in plug formation, especially in the presence of large particles at low flow rates. The results from the FIU experiments amounted to an excellent way to test the model.

The PHOENICS code offers the choice of simulating multiphase flow using Eulerian/Lagrangian or Eulerian/Eulerian formulations. As noted in Table 7, the solids are present in the FIU experiments at a volume fraction of 7.6%. At this loading the more efficient Eulerian/Eulerian method is to be used. Here, two sets (for liquid and solids) of conservation low partial differential equations for mass, momentum and energy with the laws governing the exchange between the phases have to be solved. The presence of turbulence will also require the solution of some additional equations depending on the method used to model it. This large number of equations makes the number of unknowns to be solved for at each grid point or cell extremely large and lengthy even for the most powerful computers.

An alternative that is offered by PHOENICS, is the Drift Flux method.<sup>42</sup> This is an Eulerian model which postulates that there exists one continuous medium in which there are various dispersed phase components, up to 99 components in the PHOENICS.<sup>42</sup> The mixture of the continuous and dispersed phases behave as a single fluid with properties that are referred to as the mixture properties. In this formulation only one set of differential equations is solved, to give the mixture-mean velocity at each point and time. Then separate sets of equations are solved, one for each phase, which govern its relative velocities, i.e. their differences from the mean. The later equations are algebraic ones, which are derived from the original conservation equations by neglect of the second-order terms. This entails that the relative velocities are computed by reference only to the local pressure gradients, body forces and the inter-phase friction. The volume fractions occupied by each phase, at each point and time, are calculated at the same time. This method is referred to in the PHOENICS as the Algebraic Slip method. This method is useful for simulating sedimentation and other multiphase processes, for example the separation of oil, gas and water in a centrifuge.<sup>42</sup> This formulation was used in simulating the FIU Slurry C experiment which demonstrates the process of particle settling of a simple suspension.

The geometry chosen for the FIU experiment simulations was a straight pipe with a length of 12.9 meters and a diameter of 0.0275 meters. This simple geometry was used to obtain reasonably approximate simulations quickly to test the code. More realistic geometries are being developed. After experimenting with various grid distributions along the pipeline, a computational grid composed of 60000 cells was used, 600 cells in the axial direction as shown in Figure 35, with 100 (10 X 10) cells across the radial direction, all evenly distributed.

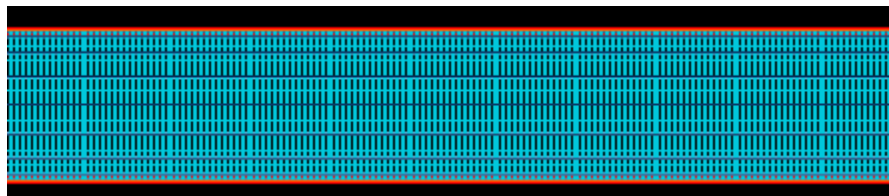


**FIGURE 35. View of the straight pipe segment ( $L = 12.9$  and  $D = 0.0275$  meters) and the grid used, enlarged 50 times in the radial direction. The grid is composed of 60,000 computational cells.**

---

A parametric study was performed to investigate particle settling and sedimentation along the transfer pipe as a function of velocity. Simulations with entrance velocities ranging from 0.5 to 2.5 meters/sec were obtained, and also included the effects of turbulence. Since the flow for all cases is in the turbulent regime, the  $k-\epsilon$  model (an eddy-viscosity model that adds two conservation equations, one for the turbulence kinetic energy  $k$ , and one for the dissipation rate  $\epsilon$ ) with wall functions were used with a 5% intensity at the entrance. The average simulation run time (CPU) was approximately 12 hours with continuous graphical convergence display. Deactivation of the graphical display will decrease the CPU time required. Calculations were performed on a work station with dual 866 Mhz Pentium III Xeon processors that was acquired in late July 2000. Run times on a

Pentium II 400 Mhz were prohibitive. Table 8 shows the entrance velocities for the cases to be presented in the coming few pages.

**TABLE 8. Entrance flow velocity for simulation cases.**

Case Number	Case 1	Case 2	Case 3	Case 4	Case 5
Flow Velocity (meters/sec.)	0.5	0.8	1.1	1.2	2.5

Center line density distributions, carrier fluid concentration, and 220  $\mu$  and 45  $\mu$  particle concentrations for the cases in Table 8 are presented in Figures 36 - 39. The concentrations in the figures are enlarged 50 times in the radial direction. The density scales from 1000 to 3147  $\text{Kg/m}^3$  while the concentrations scale from 0.0 to 1.0. The concentrations show as expected that the larger, heavier particles tend to settle fast on the bottom of the pipe especially at low flow velocities.

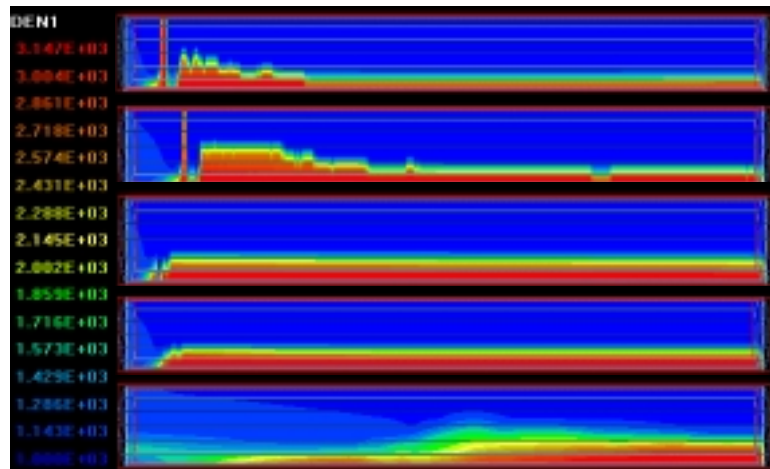


**FIGURE 36. Density distribution along the transfer pipe center line as a function of flow velocity at the entrance,  $U = 0.5, 0.8, 1.1, 1.2$  and 2.5 meters/sec.**

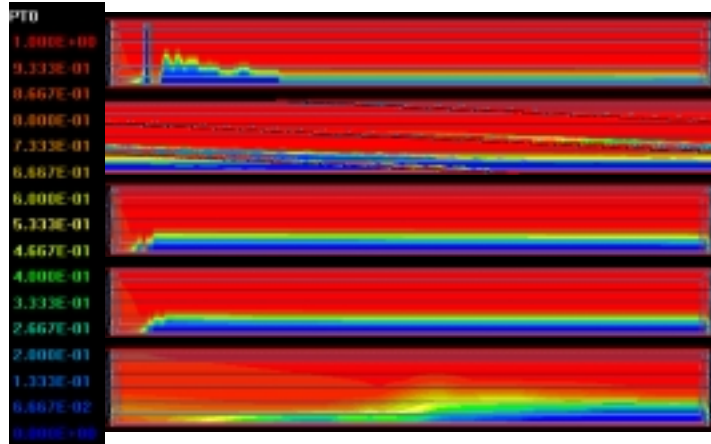


FIGURE 37. Carrier fluid concentration along the transfer pipe center line as a function of flow velocity at the entrance,  $U = 0.5, 0.8, 1.1, 1.2$  and  $2.5$  meters/sec.

---

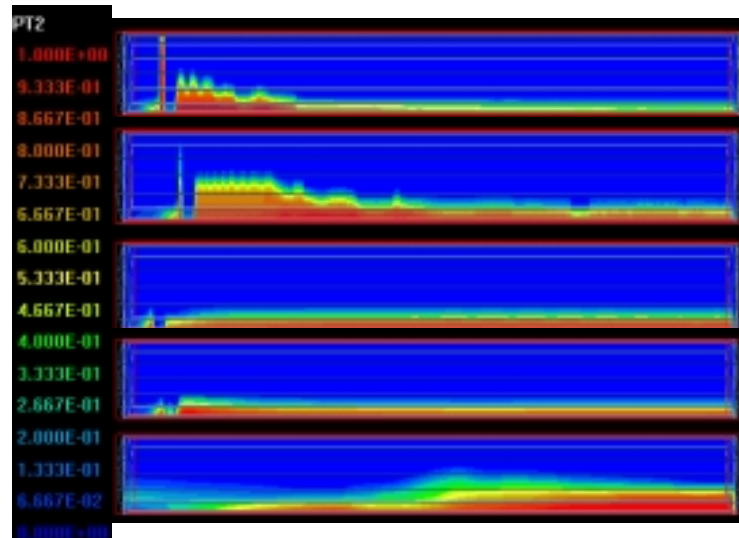
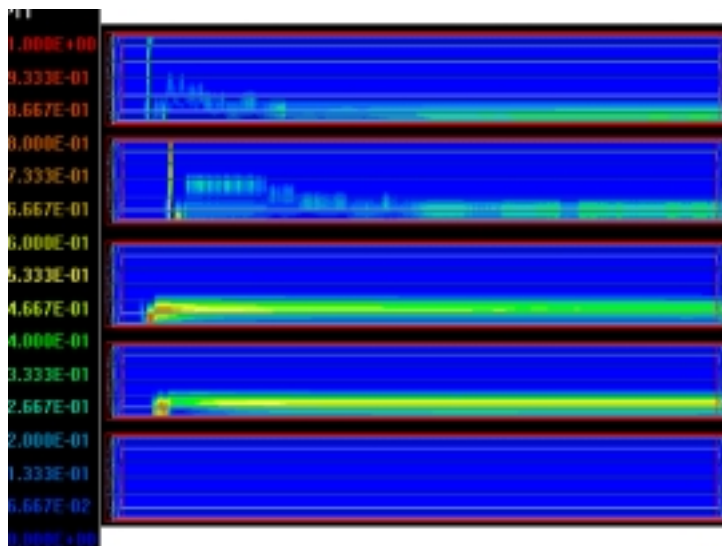


FIGURE 38.  $400 \mu$  particle concentration along the transfer pipe center line as a function of flow velocity at the entrance,  $U = 0.5, 0.8, 1.1, 1.2$  and  $2.5$  meters/sec.

---



**FIGURE 39.** 45  $\mu$  particle concentration along the transfer pipe center line as a function of flow velocity at the entrance,  $U = 0.5, 0.8, 1.1, 1.2$  and 2.5 meters/sec.

The simulations showed that flow velocities lower than 1.0 meters/sec will create a stationary bed flow that eventually causes a plug to form. Examples of possible plug formations are presented in Figures 40 and 41 for the 0.5 and 0.8 meters/sec cases. In these cases the particles accumulate along the pipeline so rapidly with the largest pileup close to the entrance. Most of the sedimentation structure was composed of the 220  $\mu$  particles. This is logical in the sense that at low flow velocities (in the range of the particle settling velocity or hindered velocity in the case of dense flows) there is not enough transport energy to suspend the particles; even in the presence of turbulence. This is due to the fact that the presence of particles will have a dampening effect on turbulence through gravity/density gradients interactions.<sup>42</sup> So, at low flow velocities, especially in the low turbulence range, the ability of turbulence to suspend solid particles especially large ones vanishes rapidly as the flow proceeds downstream to the point where the flow can become laminar. This can be added to

other factors that can affect the flow, like skin friction which causes pressure drop and loss of momentum. The change of geometry (flow terrain), i.e., bends, elbows and junctions can also create adverse effects on the flow.

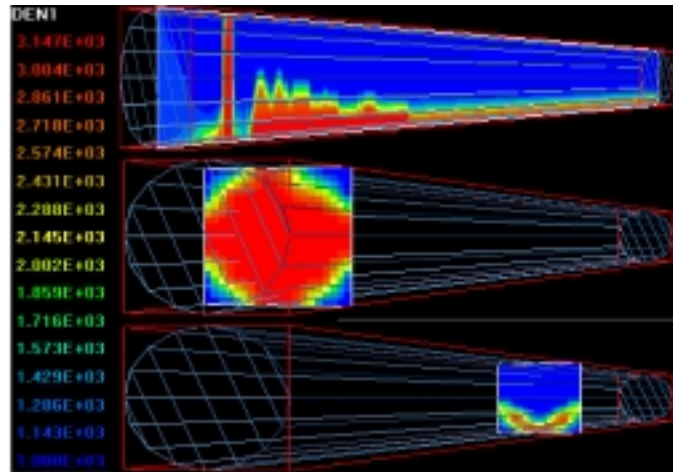


**FIGURE 40. Density distribution along the transfer pipe center line (top), across the transfer pipe line at suspected plug location (center) and at  $x = 6.45$  meters in the axial direction. Entrance velocity,  $U = 0.5$  meters/sec.**

---

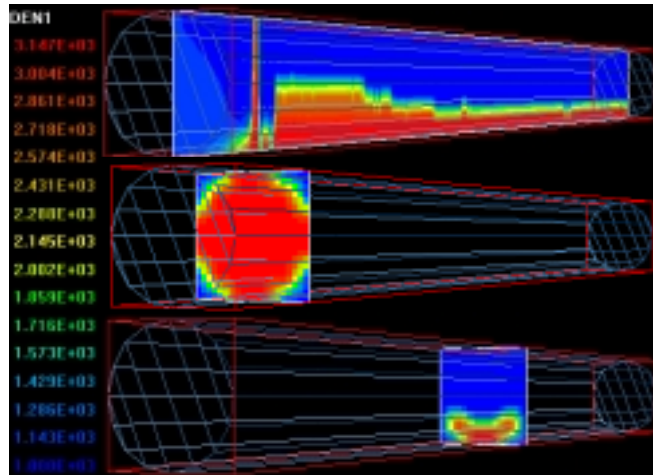


**FIGURE 41. Density distribution along the transfer pipe center line (top), across the transfer pipe line at suspected plug location (center) and at  $x = 6.45$  meters in the axial direction. Entrance velocity,  $U = 0.8$  m/sec.**

For velocities greater than 1.0 meters/sec the fluid establishes a moving bed regime where the particles move along the bottom of the transfer pipe. At still higher flow velocities the particles move much faster and stratify through the fluid layers (as for the  $45 \mu$  particle moving at 2.5 meters/sec shown in Figure 39). Predicted plug formations shown in Figures 40 and 41 suggest that flow rates with velocities larger than the largest particles (available in the fluid) settling velocity must be used to prevent stationary bed flow and the possible formation of plugs in the transfer line. The higher the velocity, the less likely a plug to form and also this implies that less water will be needed to flush the remaining particles out of the lines after the end of the pumping operation.

The researchers at FIU reported that stationary bed flow regime was established at velocities less than or equal to 0.85 meters/sec for the Slurry C experiment.<sup>37</sup> They did not give any details regarding plugging structure or specify any plug location. The model prediction

of 1.0 meters/sec minimum flow velocity exhibits a good agreement with the experimental results and even better with the Delta Q<sup>39</sup> prediction of 0.95 meters/sec bearing in mind that the differences could be in the range of experimental uncertainty and error. Other factors could contribute to small differences like the need for higher grid resolution or an entrance velocity distribution other than uniform. All of these factors will be addressed as the model development continues.

### **Project Status**

Work is continuing on both the experimental tests involving plug formation and the development of the engineering tool.

### **Conclusions**

Progress is reported on work aimed at understanding salt well pumping operations at Hanford. A laboratory-scale flow loop based on the conditions at the site was designed, constructed and calibrated with water. Flow experiments were conducted on a surrogate derived from the supernate of tank 241-SX-104. Previous experience at the site indicated the propensity of the SX-104 surrogate to form a gel based on sodium triphosphate dodecahydrate. The surrogate was characterized for gel formation at different temperatures and PLM measurements indicated the rod-like crystals. ESP calculations were used to determine the solid liquid equilibria, and heat capacity. Workers at ORNL performed initial viscosity measurements and these results indicated that the fluid was shear thickening.

Transport experiments in the flow loop revealed that the gelation of the surrogate and subsequent plug formation was a complex process that depended primarily on the linear velocity. The results obtained to date indicate that, while plugs have been formed at all flow rates examined the higher the linear velocity the longer the time needed to form the plug. Based on the observed pressure profiles, two

different plug formation mechanisms have been observed. For the same heat exchanger flow, the lower Reynolds numbers experiments result in the rapid assembly of the plug. At the highest velocity evaluated the gel assembly process is somewhat different with deposit formation and eventual assembly. The time necessary for the plug at the lowest Reynolds number was within 10% for all runs indicating the plug formed in the approximately same channel location. The heat capacity from ESP was found to agree within 9% of that measured.

Interpretation of the data is in progress using dimensionless numbers. Initial observations indicate that many of the fundamental parameters that describe the flow may exhibit changes in the vicinity of the gel formation temperature. Further laboratory experiments are needed to delineate the variation of the viscosity with shear and temperature and to understand the nucleation and growth processes associated with trisodium phosphate. Work aimed at evaluating the amounts of water necessary to ensure safe transfer and provide the basis for line flushing frequency are in progress.

Work was initiated on the development of an engineering tool that will help to prevent plug formation during the Salt Well pumping and Slurry Transfer operations at Hanford. The efforts are aimed at producing a model that will accurately predict, if, where and when a plug will form during a transfer process while taking into account the dynamic behavior of the transfer process and reflect the impact of the waste chemistry. Efficiency and ease of use to the operators and applicability to the operations at Hanford are top priorities.

The modeling approach, based on building the model using separate modules that represent a specific physical process, has started. A general Computational Fluid Dynamics system which will represent the transport module part was acquired. Initial tests using simple transport processes were performed on the transport module. Other tests addressing module sensitivity to grid distribution, initial and

boundary conditions, and initial velocity distribution at the entrance are in progress.

Simulations representing the transport process in the FIU Slurry C experiments produced good agreement with the reported results. The simulations suggested that flow rates with velocities larger than 1.0 meters/sec will produce a moving bed flow. The higher the flow rates the less likely a significant amount of particles will deposit eventually leading to the formation of a plug. This leads to the following preliminary conclusions based on the simulations results; in the absence of significant heat transfer and chemical reactions, simulations based on the more efficient and less computationally demanding Drift flux formulation for multiphase flow will produce acceptable predictions for the Slurry Transport Process.

To prevent the establishment of stationary bed flow which leads to plug formation in the pipe, a pumping flow rate producing velocities higher than the settling velocity, for the largest particle available to transport, has to be used. This will insure a minimum of moving bed flow.

Incorporation of more elaborate formulation and additional modules into the overall model are in process. This will include capabilities that will account for the complex characteristics of the waste. Modifications will include the effects of the change of solids concentration on the viscosity of the flow, phase transition, particle nucleation and growth, and chemical reactions capabilities.

### **Work Planned**

Aspects relating to line flushing and the amount of dilution water required to safely transport the surrogate (or other similar composition) waste have not yet been performed; however, the experiment reported for the highest Reynolds number flow provides an initial condition with which line flushing can be evaluated. With regard to

the dilution experiments it is expected that plug formation will proceed at a much slower rate in which case the other dimensionless numbers may become more accessible. Nucleation and growth kinetics of the rods is expected to be more tractable at the diluted conditions. In regard to the observations additional data is needed for the viscosity at both low and high shear rates.

Correlation of the experimental results with operation and process data is also needed. Here it is believed that the pressures recorded during SW operations provide the best means of comparison. Discussions with engineers at the site are in progress.<sup>43</sup>

Experiments on an additional surrogate from Hanford tank 241-U-103 are scheduled. TSP was also thought to be responsible for the plugging of the transfer line during SW pumping from this tank. Here however, it is planned to use the surrogate composition as received. Thus, the higher density phase is expected to partition into some loose solids along with the gel. A transition from gel formation to sedimentation is expected and on the case the standard framework describing particle deposition can be evaluated.

Efforts in the model development will be directed towards incorporating more physical effects. Heat transfer which causes a change in fluid viscosity as a function of temperature will be addressed first. These effects are important to prepare the model for simulations of the FIU experiments with the AN 103 slurry surrogate as the results become available. The variable viscosity will be calculated from curve fit data obtained using ESP thermodynamic model. Further improvements to the viscosity variation effects will come from the ORNL viscosity model which is expected later in 2001. Further sensitivity analysis will also be performed to estimate best combinations of grid distribution, simulation time and accuracy.

## References

32. D.A. Reynolds. May 2000. Status of waste transfers, criteria, and plans. Presented at the 3rd Saltcake Dissolution and Feed Stability Workshop, Richland, WA.  
J.R. Jewett. January 2000. Personal communication. "Tank farm information for TFA workers" and "Saltwell pumping from tank SX-104". Numatec Hanford Corporation, Richland, WA.
33. J.S. Lindner, H. Al Habbash and R.K. Toghiani. July 2000. Previous quarterly report
34. R.D. Hunt, et al. 2000. Waste preparation and transport chemistry: results of FY 2000 studies. ORNL/TM-2000/?, Oak Ridge National Laboratory, Oak Ridge, TN.
35. A. Francis, et al. June 2000. Progress report on precipitation studies of Hanford tank simulant. AEAT/R/NS/0164, AEA Technology, Harwell, UK.
36. C. Crowe, M. Sommerfeld and Y. Tsuji. 1998. Multiphase flows with droplets and particles. CRC Press LLC., Boca Raton, FL.
37. M. Ebadian, C. Lin and J.L. Xu. January 1999. Plugging and unplugging of waste transfer pipelines, preliminary data and results. FY 1998 Report, Florida International University, Center for Engineering and Applied Sciences, Miami, FL.
38. J. Tannehill, D. Anderson, R. Pletcher. 1997. Computational fluid dynamics and heat transfer. Taylor and Francis, Bristol, PA.
39. HELIX Delta Q Pipe Network Analysis Program. Helix Technology Pty. Ltd., P. O. Box 610, Morley, WA 6943, Perth, Australia.
40. Y. Onishi. and D. Trent. January 1998. TEMPEST code modifications and testing for erosion-resisting sludge simulations. Prepared for the U.S. Department of Energy, PNNL, Richland, WA.
41. Y. Onishi and K. Rechnagle. May 1999. Simulation of Hanford Tank 241-C-106 waste release into Tank 241-Y-102. Prepared for the U.S. Department of Energy, PNNL, Richland, WA.

42. R. Lyczkowski, et al. November 1994. State-of-the-art review of computational fluid dynamics modeling for fluid-solids systems. Manuscript submitted to International Symposium on Parallel Computing in Multiphase Flow Systems, ASME, Chicago, IL.
43. Multi-phase flow simulation in PHOENICS, PHOENICS Encyclopedia, POLIS, PHOENICS Online Information System. Concentrated Heat and Momentum Limited, Bakery House, Wambled Village, London SW19 5Au, UK.
44. J.E. Lamphere. August 2000. Personal communication.

*Diagnostic Field Applications Coordination and Testing Support (DFACTS)*

---

***HEPA Filter Testing***

*R. L. Cook and J. A. Etheridge*

**Introduction**

The purpose of the current work is to define a test plan and data quality objectives. We are working with the HEPA Project Work Group toward defining data quality objectives and a test plan for HEPA filter testing at DIAL.

**Work Accomplished**

After several conference calls and reviews of available literature, DIAL staff members met with Randy Brinkley and Phil McGee of the SRS HEPA Filter Test Group. The HFTG tests all HEPA filters installed at SRS (~3500 per year).

Their testing is distinctly different than that performed at the FTF at Oak Ridge:

- HFTG tests all filters mounted in place. Thus, they detect leaks both through the filter and through the housing

(which occur primarily through the gaskets). The FTF tests the filter media only.

- The HFTG tests the entire assembly at design flow rates. The FTF tests the filter at rated flow, and at 20% of rated flow.
- The HFTG uses a dispersion of poly-alpha-olefins (PAO) to challenge the filters, with a mean particle size of 0.7  $\mu\text{m}$ . The FTF uses a 0.3 mono-disperse source.

HFTG testing is based on the former DOE Order 6430.1A, the Nuclear Air Cleaning Guide Handbook, ASME 509 and 510, and the new AG-1. However, they use a site-specific procedure for testing, which reflects many years of site experience. The frequency of testing depends on the risk, and ranges from every six months (separations facility) to 18 months (closed down facility).

The test setup is fairly straightforward. A dispersion of PAO in nitrogen is introduced into the duct, where a mixing damper assures that a uniform aerosol is presented to the filter. Nominal test concentrations are 80 - 100  $\mu\text{g}/\text{l}$ . ATI instrumentation is used to determine the percent of the influent particulate in the effluent (Note: the HFTG testing produces only a relative number, not an absolute). Two tests are performed per filter, which must agree within 5%. If they do not, testing is continued until this agreement is reached. This testing is routinely performed on all filters on site, even in the most highly radioactive facilities. However, this testing does not cover other types of filters such as carbon filters used for scavenging organic contaminants.

Approximately 50 filters (1.5%) fail each year. Wetting of the filter is the primary cause of failure. Site experience is that gasket failures tend to cause results which are near the acceptance rate, while compromising the media generally gives much poorer results.

DIAL staff also visited the Filter Test Facility (FTF) at Oak Ridge. David Crosby, who is an ATI employee responsible for setting up and bringing the FTF into operation, showed the team the facility and explained its operation. The FTF tests HEPA filters (including those for gas masks) for all of the DOE facilities and some military sites as well as private companies. They test for efficiency, pressure, flow, and also for general quality problems such as proper gluing of gaskets, workmanship, etc. During the average year they fail about 15% of the filters tested. The major reasons are bad gaskets, improper labeling, and poor workmanship. During the past year approximately 30% of the filters failed. This was because one manufacturer produced a lot of filters in which the glue holding the gaskets did not set up properly.

They use DOP as the challenge agent. It gives a much narrower particle size distribution which they can control. It was noted that it was used in a controlled environment (no plastics) because it would dissolve some materials. They use the DOP to produce an aerosol with mean particle size of 0.2 microns (count diameter) with a mass/geometric diameter of 0.3 microns. The loading at the filter input is 20 to 80  $\mu\text{g}/\text{l}$  and they measure the loading after the filter with a photometer. The input particle size is measured using a polarizer and manually adjusted to the 0.2 requirement. They get a percentage penetration which is used to either pass or fail the filter. The photometer is apparently calibrated to measure that specific particle size.

It was interesting that they tested at 100% and 20% of rated flow. If there is not a linear relation between the percent penetration at 20% and that at 100%, then there is a problem. It was stated that pinholes, for example, could cause the penetration to be nonlinear with flow rate (penetration at 20% not equal 1/5 of the penetration at 100%).

## **Work Planned**

DIAL has written a preliminary data quality objectives document which is currently being reviewed by the other members of the HEPA group. DIAL will use the final form of this document, along with other input from the group, for developing a test program for HEPA filters.

## **Nomenclature**

DOP

FTF

HEPA

HFTG